FOXC2 and fluid shear stress stabilize postnatal lymphatic vasculature

Amélie Sabine,[1] Esther Bovay,[1] Cansaran Saygili Demir,[1] Wataru Kimura,[2] Muriel Jaquet,[1] Yan Agalarov,[1] Nadine Zangger,[3] Joshua P. Scallan,[4] Werner Graber,[5] Elgin Gulpinar,[6] Brenda R. Kwak,[7] Taija Mäkinen,[8] Inés Martinez-Corral,[9] Sagrario Ortega,[9] Mauro Delorenzi,[3,10] Friedemann Kiefer,[11] Michael J. Davis,[4] Valentin Djonov,[5] Naoyuki Miura,[2] and Tatiana V. Petrova[1,12]

[1]Department of Fundamental Oncology, Centre Hospitalier Universitaire Vaudois and University of Lausanne, Epalinges, Switzerland. [2]Hamamatsu University School of Medicine, Hamamatsu, Japan. [3]SIB Swiss Institute of Bioinformatics, Lausanne, Switzerland. [4]University of Missouri, Columbia, Missouri, USA. [5]Institute of Anatomy, University of Bern, Bern, Switzerland. [6]Harvard College, Cambridge, Massachusetts, USA. [7]Department of Pathology and Immunology and Department of Medical Specializations – Cardiology, University of Geneva, Geneva, Switzerland. [8]Department of Immunology, Genetics and Pathology, Uppsala University, Uppsala, Sweden. [9]Spanish National Cancer Research Centre, Madrid, Spain. [10]Ludwig Center for Cancer Research, University Lausanne, Lausanne, Switzerland. [11]Max Planck Institute for Molecular Biomedicine, Münster, Germany. [12]Swiss Cancer Research Institute, École Polytechnique Fédérale de Lausanne, Lausanne, Switzerland.

Biomechanical forces, such as fluid shear stress, govern multiple aspects of endothelial cell biology. In blood vessels, disturbed flow is associated with vascular diseases, such as atherosclerosis, and promotes endothelial cell proliferation and apoptosis. Here, we identified an important role for disturbed flow in lymphatic vessels, in which it cooperates with the transcription factor FOXC2 to ensure lifelong stability of the lymphatic vasculature. In cultured lymphatic endothelial cells, *FOXC2* inactivation conferred abnormal shear stress sensing, promoting junction disassembly and entry into the cell cycle. Loss of FOXC2-dependent quiescence was mediated by the Hippo pathway transcriptional coactivator TAZ and, ultimately, led to cell death. In murine models, inducible deletion of *Foxc2* within the lymphatic vasculature led to cell-cell junction defects, regression of valves, and focal vascular lumen collapse, which triggered generalized lymphatic vascular dysfunction and lethality. Together, our work describes a fundamental mechanism by which FOXC2 and oscillatory shear stress maintain lymphatic endothelial cell quiescence through intercellular junction and cytoskeleton stabilization and provides an essential link between biomechanical forces and endothelial cell identity that is necessary for postnatal vessel homeostasis. As *FOXC2* is mutated in lymphedema-distichiasis syndrome, our data also underscore the role of impaired mechanotransduction in the pathology of this hereditary human disease.

Introduction

Active and complex signaling is involved both in the growth of new vessels and their stabilization and maintenance. Blood vessel stabilization encompasses proliferation arrest, restoration of the vascular barrier function, and acquisition of mural cell coverage. These properties need to be maintained for the lifetime of the organism to ensure optimal perfusion and tissue homeostasis (1). Laminar blood flow is an important vessel-stabilizing factor: it contributes to the termination of angiogenic signaling and vessel specialization through oxygenation of tissues and mechanoregulation of endothelial cells (2). In contrast, disturbed blood flow induces endothelial dysfunction, involving proinflammatory signaling, enhanced proliferation, and apoptosis, which ultimately lead to pathological responses like the formation of atherosclerotic lesions (2).

In addition, blood vessel stability and integrity require mature cell-cell junctions and mural cell coverage. Molecular players implicated in the regulation and maintenance of vascular stability include ANG1/TIE2, FGF, Notch, S1P, PDGF-β and TGF-β signaling, extracellular matrix, and proteases. Important progress has already been achieved in our understanding of the molecular regulation of blood vessel stability (3). However, little is known about the processes involved in stabilization of the lymphatic vasculature, despite its key role in normal homeostasis and in a variety of pathological conditions, such as tumor metastasis and chronic inflammation (4).

The lymphatic vasculature comprises two structurally and functionally distinct compartments: capillaries and collecting vessels. Interstitial fluid and immune cells enter via discontinuous intercellular junctions in lymphatic capillaries and are transported by collecting vessels to lymph nodes as a result of coordinated contractions of vascular smooth muscle cells, valve opening, and closure cycles and pressure gradients from surrounding tissues (5). Such functional separation is critically important for optimal lymphatic function (6, 7); yet how it is maintained throughout life remains to be defined.

Here, we interrogated the molecular mechanisms of postnatal collecting lymphatic vessel maintenance. We showed that collecting lymphatic vessel function requires continuous expression of the forkhead transcription factor FOXC2 in areas of disturbed flow, such as lymphatic valves. FOXC2 controls endothelial cytoskeleton organization and thus ensures cell-cell junction stability, endothelial integrity, and cell-cycle arrest under disturbed flow conditions.

Authorship note: Esther Bovay and Cansaran Saygili Demir contributed equally to this work.
Conflict of interest: The authors have declared that no conflict of interest exists.
Submitted: December 11, 2014; **Accepted:** August 13, 2015.
Reference information: *J Clin Invest*. 2015;125(10):3861–3877. doi:10.1172/JCI80454.

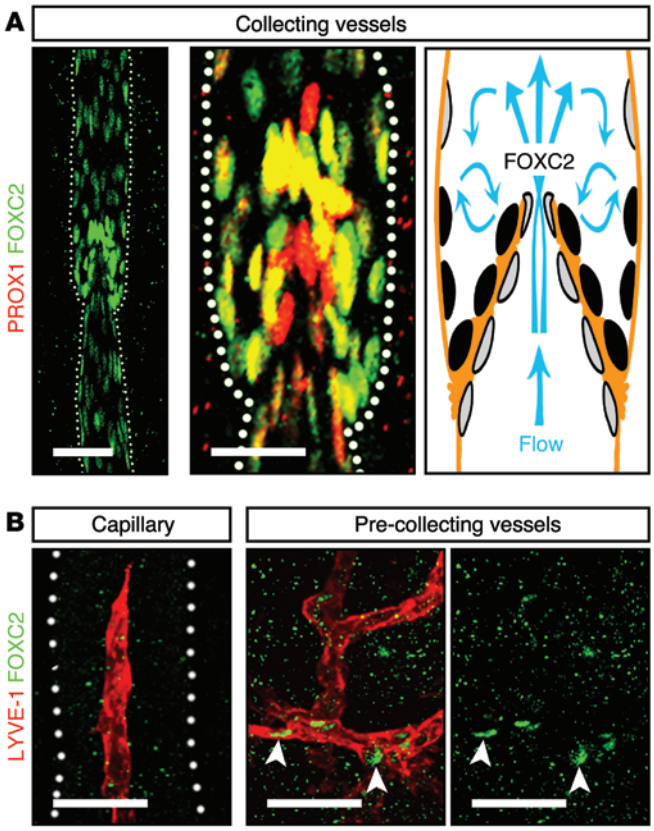

Figure 1. FOXC2 expression pattern in postnatal lymphatic vessels. (**A**) In P8 mesenteric lymphatic vessels FOXC2 (green) is highly expressed in the valve sinuses subjected to recirculating flow, while only low levels are found on the upstream luminal part of the valve exposed to laminar shear stress. PROX1 (red) is strongly expressed on both sides of the valve leaflet. (**B**) FOXC2 levels are low in P8 intestinal lymphatic capillaries, and only occasional FOXC2$^+$ cells are detected in submucosal pre-collecting vessels. Intestinal villus is outlined with a dotted line. The arrowheads indicate FOXC2$^+$ cells. Scale bars: 50 μm.

We further showed that FOXC2 secures cell dormancy by blocking proliferation mediated by the mechanosensitive Hippo pathway transcriptional coactivator TAZ. Our work establishes a general principle of postnatal lymphatic vascular organization in which FOXC2 plays a central role in maintaining collecting vessel quiescence and stability, notably in valve areas, by linking shear stress responses to cell junction stabilization and cell-cycle arrest. *FOXC2* is mutated in lymphedema-distichiasis, a debilitating human disease, characterized by lymphedema of the lower limbs and valve defects (8). Our work now provides a robust mouse model, in which the rapid onset of lymphatic vascular dysfunction makes it especially suitable for therapeutic preclinical studies.

Results

FOXC2 is highly expressed in areas of flow recirculation. FOXC2 plays an important role in the initiation of embryonic collecting lymphatic vessel formation (7, 9). We found that FOXC2 continues to be highly expressed in the postnatal collecting lymphatic vessels (Figure 1A). In agreement with the previously demonstrated induction of FOXC2 expression by oscillatory shear stress (OSS) in vitro (10), FOXC2 levels were highest in endothelial cells of the valve sinuses (Figure 1A), which are exposed to disturbed flow patterns (11). FOXC2 was low in the parts of the valve leaflets exposed to laminar shear stress (Figure 1A) and in capillary or pre-collecting vessel lymphatic endothelial cells (LECs) (Figure 1B), whereas cells in lymphangions expressed intermediate levels of FOXC2 (Figure 1A).

FOXC2 regulates shear stress–induced quiescence and survival. To analyze whether FOXC2 regulates responses to disturbed flow, we studied LECs cultured under static or oscillatory flow conditions, which mimic disturbed flow (11). We first analyzed the transcriptome of LECs subjected to OSS, in the presence or absence of FOXC2 (control or *FOXC2*^{KD} cells, respectively), and compared them to cells cultured under static conditions (Figure 2A and Supplemental Figure 1A; supplemental material available online with this article; doi:10.1172/JCI80454DS1). In control cells, OSS affected the expression of over 800 genes (FDR < 0.05, Figure 2B and see validation by qPCR in Supplemental Figure 1, B–D). Analysis of Kyoto Encyclopedia of Genes and Genomes (KEGG) pathways (12, 13) revealed important rewiring of LEC metabolism by OSS, as demonstrated by activation of steroid and terpenoid backbone biosynthesis, glutathione metabolism, and the pentose phosphate pathway (Supplemental Table 1). Surprisingly, cell cycle and mitosis pathways were the most significantly repressed KEGG pathways, as evidenced by a concerted decreased expression of genes associated with cell-cycle progression (Supplemental Table 1). This result was unexpected, as disturbed flow is a known inducer of proliferation in blood endothelial cells (BECs) (11).

FOXC2 inactivation modified the expression of 35% of the shear stress–responsive genes, demonstrating that FOXC2 regulates a significant proportion of LEC shear stress transcriptional responses (Figure 2B). *FOXC2*^{KD} cells demonstrated an abnormal shear stress response, as observed by reduced expression of known shear stress–responsive genes, such as *eNOS* and *CX37* (refs. 10, 14, and Supplemental Figure 1, B and C). Most strikingly, cell-cycle progression genes were no longer repressed by OSS in *FOXC2*^{KD} cells, suggesting that cells fail to undergo growth arrest (Figure 2, C and D, and Supplemental Figure 1, E and F). In contrast, *FOXC2* knockdown did not affect OSS-dependent suppression of the genes related to immune responses or OSS-dependent induction of the genes related to cholesterol biosynthesis (Figure 2, C and D), suggesting a specific role of FOXC2 in the OSS-induced downregulation of cell proliferation.

We next analyzed LEC proliferation in static and OSS conditions by staining for the proliferation marker Ki67 (Figure 3, A and B). Low but detectable proliferation of LECs in static conditions was significantly decreased by OSS (Figure 3B). Surprisingly, but in agreement with the transcriptome analyses (Figure 2, C and D), *FOXC2*^{KD} cells displayed a 10-fold increase in the number of Ki67$^+$ cells in OSS when compared with that of control cells. This finding was further confirmed by the analysis of DNA synthesis and the use of a second *FOXC2* siRNA (Supplemental Figure 2, A–C).

In BECs, disturbed flow induces not only cell proliferation, but also cell death (11). To study whether FOXC2 regulates cell survival, we stained cells for the apoptosis marker activated caspase-3. However, we could not detect any apoptotic cells under OSS (data not shown), likely due to their rapid elimination by the flow. To overcome this limitation, we performed a time-lapse microscopy analysis. We found that OSS induced the death and quick detachment of some

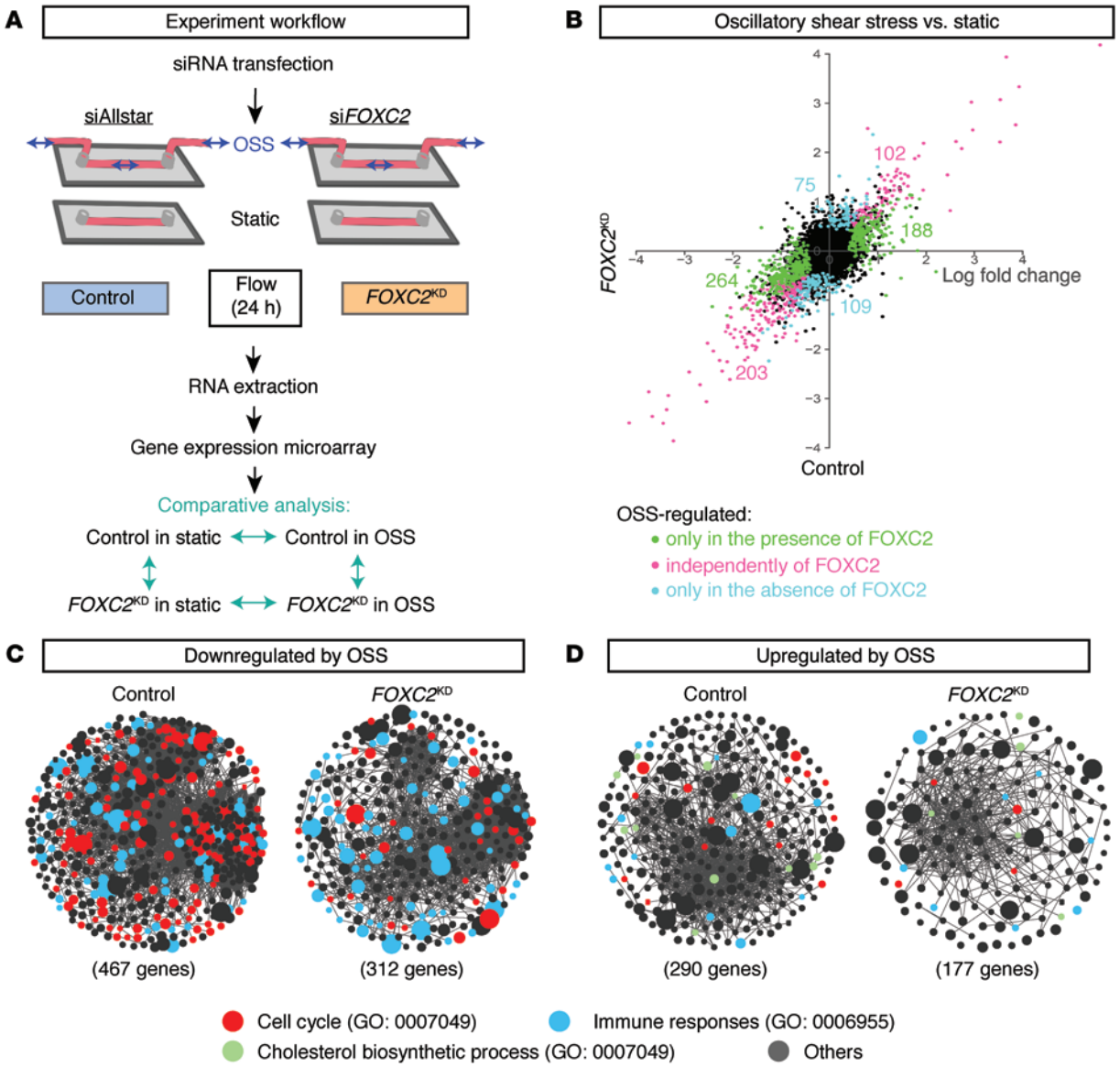

Figure 2. FOXC2 represses a proliferative genetic program in LECs under disturbed flow conditions. (**A**) Flowchart of the experiments for in vitro *FOXC2* knockdown in LECs, shear stress treatment, and gene expression analysis. (**B**) Scatter plot of global changes in gene expression induced by OSS in control and *FOXC2*^{KD} cells. Colored dots indicate transcripts changed in the indicated conditions (n = 2; regularized t test, FDR < 0.05); black dots indicate stable transcripts. Downregulated and upregulated genes appear on the left and right sides of the plot, respectively. The numbers of transcripts significantly regulated in both control and *FOXC2*^{KD} cells (pink), only in control cells (green), and only in *FOXC2*^{KD} cells (blue) are indicated on the plot. (**C** and **D**) Protein interaction networks for genes (**C**) repressed or (**D**) induced by OSS in control or *FOXC2*^{KD} cells. The number of genes for each condition is indicated. Genes associated with cell cycle, immune responses, or cholesterol biosynthesis are highlighted, with the corresponding colored dots on the networks. Dot size reflects the degree of changes for each transcript. Data are obtained from 2 independent experiments (see also Supplemental Figure 1).

control cells (Figure 3, C and D, and Supplemental Videos 1 and 2). Importantly, we observed increased proliferation of *FOXC2*^{KD} cells under OSS, which was also accompanied by increased cell death (Figure 3, C and D, and Supplemental Videos 3 and 4).

Endothelial cells actively migrate during sprouting (lymph) angiogenesis, whereas the motility of endothelial cells in quiescent vessels is reduced, which is important for overall vessel stability (3). To evaluate whether FOXC2 plays a role in LEC motility, we tracked the movement of control and *FOXC2*^{KD} cells in the presence and absence of OSS. LECs were highly motile under static conditions and became immobilized under OSS (Figure 3E and Supplemental Videos 5 and 6), suggesting stabilization of the endothelial monolayer. In contrast, although *FOXC2*^{KD} LECs were less motile in static conditions, they migrated more in OSS (Figure 3E, Supplemental Figure 2D, and Supplemental Videos 7 and 8).

Thus, we conclude that in LECs OSS triggers growth and motility arrest, which may protect vessel integrity by reducing the cell turnover (Figure 3F). Of interest, although further studies are warranted, our data suggest that LECs respond differently to disturbed flow in comparison to BECs (11). Most importantly, FOXC2 plays a key role in such LEC responses, suggesting that FOXC2 acts as a guardian of LEC quiescence and survival in disturbed flow conditions.

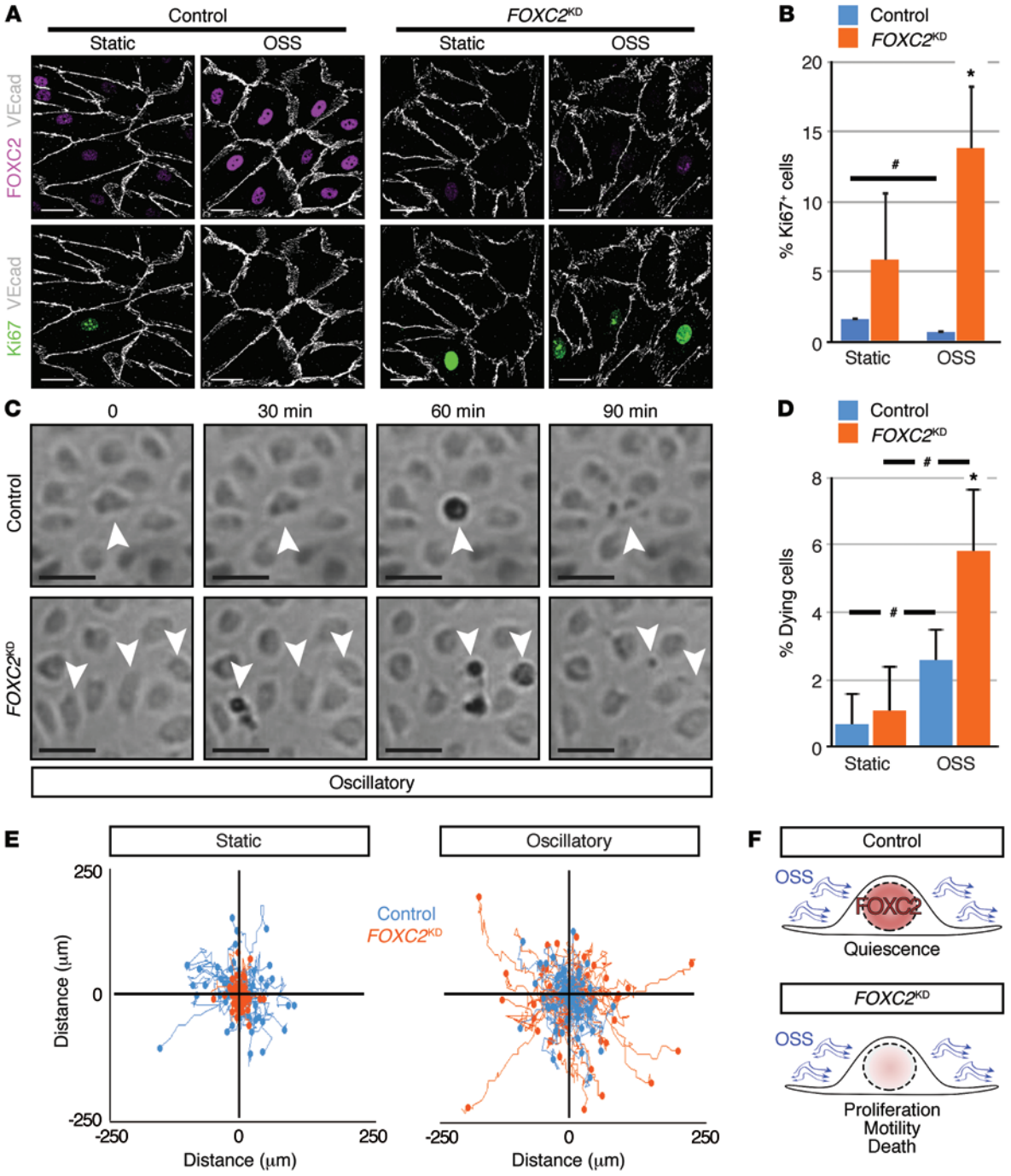

Figure 3. FOXC2 controls the quiescent state and survival of LECs under disturbed flow conditions. (**A**) *FOXC2*^{KD} cells proliferate more under OSS. Staining for FOXC2 (pink), VE-cadherin (white), and proliferation marker Ki67 (green). (**B**) Quantification of Ki67^{+} cells in **A** in the indicated conditions. (**C**) *FOXC2*^{KD} cells have an increased death rate under OSS. Time-lapse microscopy images of control and *FOXC2*^{KD} cells. White arrowheads indicate dying cells. (**D**) Quantification of dying cells in **C** over 4 hours of recording. (**E**) Increased motility of *FOXC2*^{KD} cells under OSS. Cell trajectory plots of individual control (blue) or *FOXC2*^{KD} (orange) cells in static or OSS conditions. (**F**) Scheme showing control or *FOXC2*^{KD} cell phenotype under OSS. Control cells become quiescent, while *FOXC2*^{KD} cells show increased proliferation, motility, and death. Scale bars: 10 μm. $n = 3$; more than 50 cells scored per condition; 2-tailed unpaired Student's *t* test; $^{\#}P < 0.05$ (static vs. OSS), $^{*}P < 0.05$ (control vs. *FOXC2*^{KD}) (see also Supplemental Figure 2 and Supplemental Videos 1–8).

FOXC2 controls cell-cell junction and cytoskeleton organization in a cell-autonomous manner. Given the known relevance of cell-cell junctions in contact inhibition of growth (15), we next analyzed whether FOXC2 regulates lymphatic endothelial intercellular junctions. As previously described (16), control LECs displayed mostly linear intercellular junctions in static conditions (Figure 4, A–C). Exposure to OSS resulted in the transformation of such linear junctions into overlapping contact sites, often assembled into a complex reticular adherens network (Figure 4, A–C), which has been previously described in quiescent BECs (17). Taken together with the fact that OSS induces LEC quiescence and motility arrest, this observation suggests that OSS stabilizes cell-cell junctions. Induc-

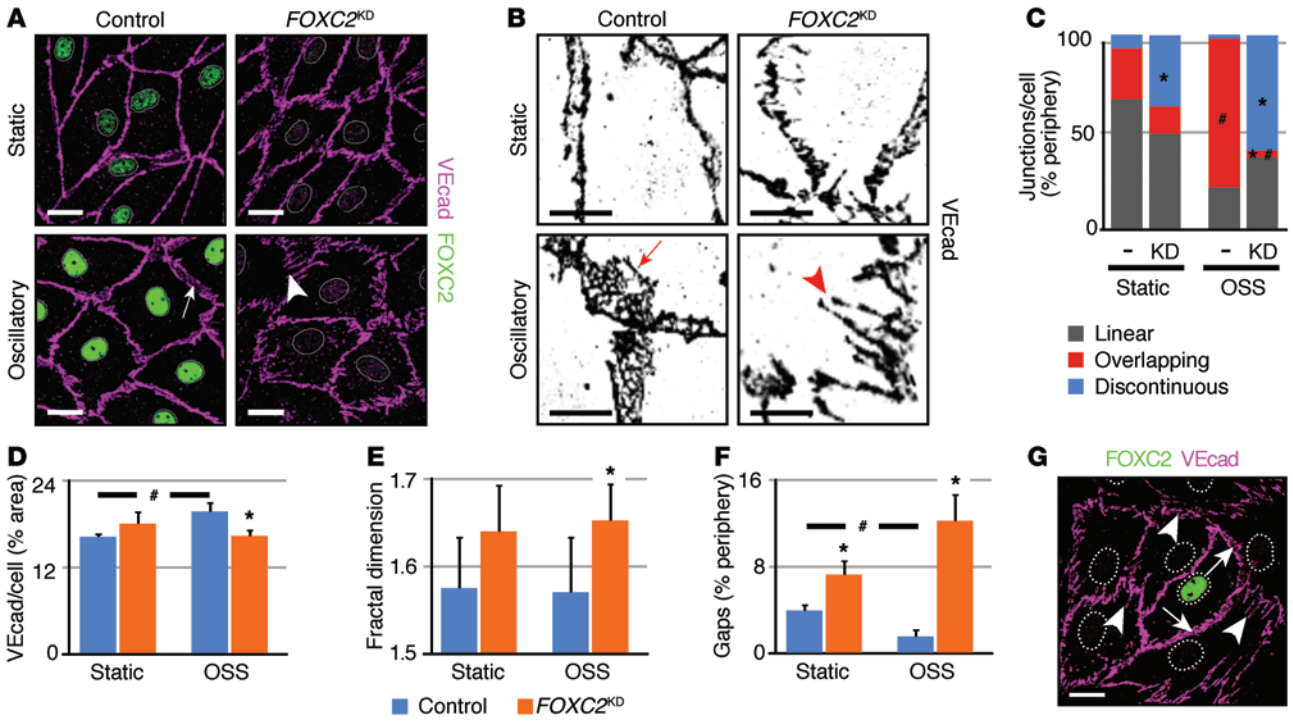

Figure 4. FOXC2 and OSS control adherens cell-cell junction integrity. (**A**) Staining of control and *FOXC2*^{KD} cells for FOXC2 (green) and VE-cadherin (pink). The arrow indicates an overlapping junction induced by OSS; the arrowhead indicates a zigzag-like junction induced by FOXC2 depletion. Cell nuclei are outlined by white lines. (**B**) High-magnification images of VE-cadherin junctions (black) show the formation of reticular structures (red arrow) in control cells under OSS, while *FOXC2*^{KD} cells have mostly discontinuous and thin cell-cell contacts (red arrowhead). (**C**) Quantification of adherens cell-cell junction types in control and *FOXC2*^{KD} cells. VE-cadherin^{+} junctions were classified as linear (exemplified by control/static image in **B**), overlapping (exemplified by control/oscillatory image in **B**), or discontinuous (exemplified by *FOXC2*^{KD}/oscillatory image in **B**). The proportion of each junction type was determined for the entire cell periphery. (**D**) OSS increases VE-cadherin^{+} junctional area in control but not in *FOXC2*^{KD} LECs. (**E**) Increased junction complexity in *FOXC2*^{KD} cells, as indicated by increased fractal dimension of the VE-cadherin organization. (**F**) Increased number of VE-cadherin^{-} gaps in *FOXC2*^{KD} LECs. (**G**) FOXC2-dependent cell-cell junction remodeling is cell autonomous. The isolated FOXC2^{+} cell has continuous junctions (arrows), while the neighboring *FOXC2*^{KD} cells have zigzag junctions (arrowheads). Staining for FOXC2 (green) and VE-cadherin (pink). Cell nuclei are outlined with dashed white lines. Scale bars: 10 μm (**A** and **G**); 5 μm (**B**). $n = 3$; more than 50 cells scored per condition; 2-tailed unpaired Student's t test; $^{\#}P < 0.05$ (static vs. OSS), $^{*}P < 0.05$ (control vs. *FOXC2*^{KD}) (see also Supplemental Figure 3, A and B).

tion of overlapping cell-cell junctions and growth arrest was specific to OSS, as LECs under laminar shear stress displayed mostly linear cell-cell junctions and a somewhat increased proliferation (Supplemental Figure 2, E and F). *FOXC2* knockdown resulted in partial disruption of the continuous VE-cadherin staining pattern in LECs under static conditions, which was transformed into a zigzag-like junctional structure (Figure 4, A–C). Importantly, this phenotype was further strongly potentiated by OSS (Figure 4, A–C). There was a general reduction of the junctional area (Figure 4D) associated with an increased junction complexity (Figure 4E) and an increased number of interendothelial gaps (Figure 4F). Staining for β-catenin, which links VE-cadherin to the actin cytoskeleton, and a marker of tight junctions, ZO-1, revealed similar linear or zigzag-like patterns of junctions in control and *FOXC2*^{KD} cells, respectively (Supplemental Figure 3, A and B). Importantly, in partial knockdown experiments, FOXC2^{+} cells maintained overlapping junctions, whereas surrounding FOXC2^{-} cells had zigzag junctions, demonstrating that FOXC2 protects junctions cell autonomously and not in a paracrine manner (Figure 4G).

We further examined organization of the actin cytoskeleton in control and *FOXC2*^{KD} cells. As previously described, cells under static conditions had only a thin rim of cortical actin, and OSS induced the formation of thick cortical actin stress fibers (ref. 10 and Figure 5A). The density of actin fibers was increased upon *FOXC2* knockdown in static conditions, and this was further drastically enhanced under OSS (Figure 5A). Staining for the phosphorylated myosin light chain 2 (pMLC2), an indicator of actomyosin contractility, was rather weak in control cells, even under OSS (Figure 5A). In contrast, actin fibers were associated with increased pMLC2 in *FOXC2*^{KD} cells (Figure 5A), suggesting greater contractile forces in these cells under disturbed flow conditions. Further analyses demonstrated a close association of VE-cadherin with actin stress fibers in *FOXC2*^{KD} zigzag cell-cell junctions (Supplemental Figure 3C), suggesting that stress fiber contractility on each side of the junction causes VE-cadherin zigzag patterning. Therefore, it is possible that junction stability is maintained by a FOXC2-dependent fine-tuning of the intercellular tensional cytoskeletal forces and regulation of RhoA/ROCK/MLC signaling.

We also analyzed the distribution of vinculin, which anchors actin fibers to focal adherens junctions between cells or focal adhesions to the cell matrix. Vinculin is a mechanosensing protein, which controls force-dependent junction remodeling by integrating the cytoskeleton tensional forces and protecting junc-

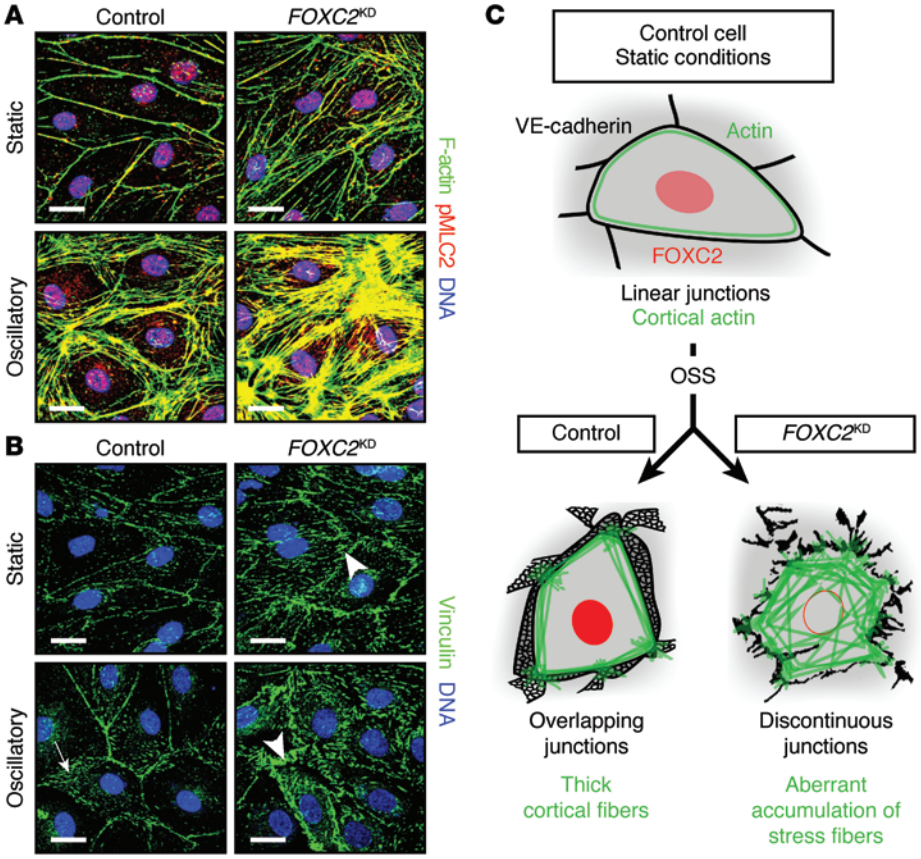

Figure 5. FOXC2 and OSS control actin cytoskeleton organization. (**A**) Abnormal organization and increased contractility of actomyosin in *FOXC2*^{KD} cells is potentiated by OSS. Staining for F-actin (green) and pMLC2 (red). (**B**) FOXC2 depletion and OSS enhance vinculin recruitment to the intercellular junctions (arrowheads in *FOXC2*^{KD} vs. arrow in control cells). Staining for vinculin (green). (**C**) Scheme for the role of FOXC2 in remodeling of LEC junctions under shear stress. OSS induces cortical stress fibers and overlapping reticular junctions, whereas *FOXC2* inactivation leads to aberrant accumulation of highly contractile stress fibers, junction disruption, and formation of interendothelial gaps (see also Supplemental Figure 3C). Scale bars: 10 μm.

tions from disrupting under such forces (18). Vinculin levels were augmented in junctional areas between *FOXC2*^{KD} cells when compared with control cells, suggesting higher intercellular traction forces and loss of junction integrity (Figure 5B).

In conclusion, LECs normally adapt to oscillatory flow by reinforcing cell-cell junctions. Such increased overlapping interaction surface, associated with cortical actin cytoskeleton at the cell-cell junction, is likely important for providing resistance to mechanical stress. Loss of FOXC2 prevents the formation of overlapping junctions and leads to profound remodeling of the cell cytoskeleton, increased actomyosin contractility, and formation of discontinuous cell-cell junctions, prone to disruption when subjected to mechanical forces (Figure 5C). Thus, we propose that FOXC2 is necessary for stabilization of cell-cell junctions and the ability of cells to withstand mechanical stress.

FOXC2 buffers YAP1/TAZ signaling in LECs. FOXC2-depleted LECs respond to OSS by cytoskeleton hypercontractility, intercellular junction disruption, aberrant proliferation, and, ultimately, increased cell death. We hypothesized that the observed cytoskeletal and junctional changes relieve the contact inhibition, thus initiating proliferation of *FOXC2*^{KD} cells. Mechanotransduction regulates cell proliferation via cytoplasmic versus nuclear localization of YAP1/TAZ transcriptional coactivators, which can also be sequestered by junction molecules, such as catenins and angiomotins (19, 20). Contact inhibition of cell growth is triggered through inactivation of YAP1/TAZ, whereas low cell density or loss of cell-cell contacts induces nuclear translocation of YAP1/TAZ and subsequent activation of cell cycle (15, 21).

Analyses of genes regulated by OSS in the presence or absence of FOXC2 revealed that *FOXC2*^{KD} cells expressed higher levels of YAP1/TAZ target genes *CTGF*, *CYR61*, and *ANKRD1* (22), and this effect was further potentiated under OSS (Figure 6A), suggesting that FOXC2 restricts the activation of YAP1/TAZ signaling by oscillatory flow. Staining of LECs demonstrated that OSS increased nuclear localization of YAP1/TAZ in both control and *FOXC2*^{KD} cells (Figure 6, B and C). However, while YAP1/TAZ was detected in control cell-cell junctions, it was mostly nuclear and absent from junctions in *FOXC2*^{KD} cells (Figure 6B and Supplemental Figure 4A). These results were in line with in vivo analyses, which demonstrated nuclear localization of TAZ and YAP1 in lymphatic valves (Figure 6D and data not shown). To study whether YAP1/TAZ play a functional role in *FOXC2*^{KD} cells, we silenced *YAP1* and *TAZ* in FOXC2-depleted cells and analyzed cell proliferation in OSS by staining for Ki67. We found that *YAP1/TAZ* knockdown significantly reduced the hyperproliferation of *FOXC2*^{KD} cells (Figure 6E and Supplemental Figure 4B). Surprisingly, knockdown of *YAP1* had no effect on the number of Ki67^{+} cells (Figure 6F), despite significant YAP1 downregulation (Supplemental Figure 4C). In contrast, depletion of TAZ with 2 different siRNAs abrogated the aberrant proliferation of *FOXC2*^{KD} cells, without affecting junction organization (Figure 6G and Supplemental Figure 4, D–F). Interestingly, TAZ inactivation alone, in addition to reducing the expression of the TAZ target genes *CTGF*, *CYR61*, and *ANKRD1* (Supplemental Figure 4G), was sufficient to decrease the proliferation of LECs in static conditions (Supplemental Figure 4H).

Collectively, these data highlight the role of cell-cell junctions and cytoskeleton organization in the control of LEC quiescence

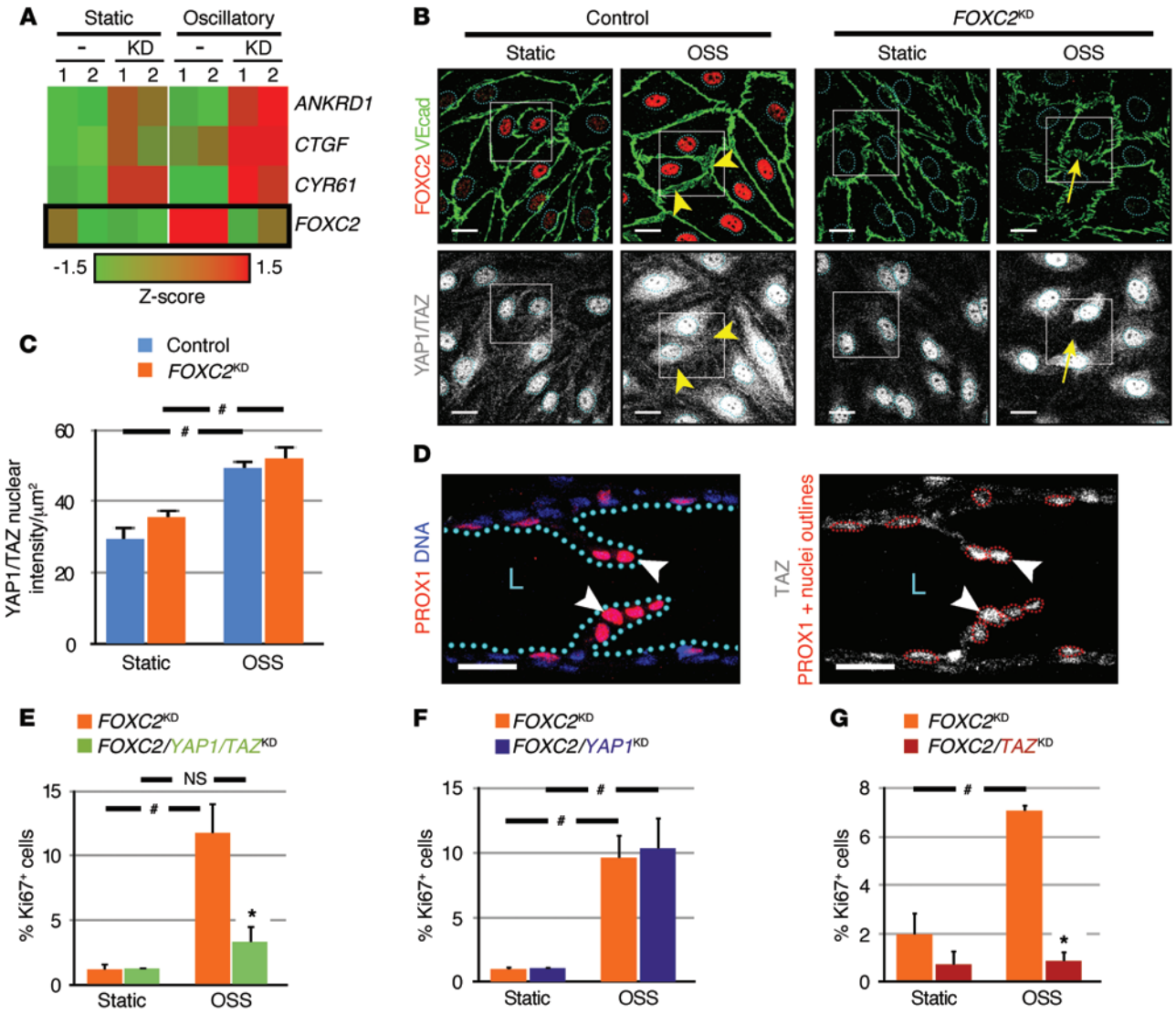

Figure 6. FOXC2 restricts YAP1/TAZ signaling in LECs under disturbed flow. (**A**) YAP1/TAZ target genes are over induced in the absence of FOXC2. Heat map for the indicated genes (red, increased expression; green, decreased expression). KD, *FOXC2*^{KD}. (**B**) YAP1/TAZ accumulate in the nuclei of both control and *FOXC2*^{KD} cells subjected to OSS. Staining for FOXC2 (red), VE-cadherin (green), and YAP1/TAZ (white). Only control cells showed YAP1/TAZ in the cell-cell junctions (arrowheads), whereas it was mostly absent from *FOXC2*^{KD} VE-cadherin^{+} areas (arrows). Nuclei are outlined with dashed blue lines. High-magnification images of the boxed areas are shown in Supplemental Figure 4A. (**C**) Corresponding quantification of YAP1/TAZ intensity per nucleus μm^2. (**D**) Nuclear localization of TAZ in the lymphatic valves. Staining for PROX1 (red) and TAZ (white) of P7 collecting mesenteric vessels. Lymphatic valve cells were identified by high PROX1 expression (arrowhead). The vascular lumen (L) is outlined with a dotted blue line and DNA is stained in blue (left), and PROX1^{+} nuclei are outlined with a dotted red line (right). (**E**–**G**) Depletion of TAZ, but not YAP1, in *FOXC2*^{KD} cells reverses hyperproliferation under OSS. Quantification of Ki67^{+} cells in *FOXC2*^{KD} (orange) and (**E**) *FOXC2/YAP1/TAZ* knockdown (green) cells, (**F**) *FOXC2/YAP1* knockdown (purple) cells, or (**G**) *FOXC2/TAZ* knockdown (red) cells. Scale bars: 10 μm (**B**); 20 μm (**D**). $n = 3$ in **C** and **E**; $n = 2$ in **F** and **G**; more than 50 cells scored per condition; 2-tailed unpaired Student's t test; $^{\#}P < 0.05$ (static vs. OSS), $^{*}P < 0.05$ (control vs. *FOXC2*^{KD}) (see also Supplemental Figure 4). NS, not significant.

in response to OSS. These results suggest that, while OSS is able to increase YAP1/TAZ nuclear translocation, FOXC2 efficiently blocks the pro-proliferative effect of TAZ and thus safeguards LEC quiescence and survival under disturbed flow conditions.

FOXC2 is essential for postnatal lymphatic vascular function. To assess the role of FOXC2 in the postnatal lymphatic vasculature in vivo, we generated a lymphatic endothelial-specific, tamoxifen-inducible loss-of-function mouse model (*Foxc2*$^{fl/fl}$ *Prox1*-Cre^{ERT2} [*Foxc2*^{lecKO}]) (Supplemental Figure 5, A–D). Inactivation of *Foxc2* led to fully penetrant mortality, with the onset varying from a few days during early postnatal inactivation to up to 5 months in adult mice (Figure 7A and data not shown). Macroscopic analyses demonstrated development of chylous ascites and chylothorax in *Foxc2*^{lecKO} animals (Figure 7B). Further examination revealed dilated submucosal lymphatic vessels in the small intestine and chyle-filled lymphatic vessels in the cecum, which normally does not receive chyle because of efficient fat absorption in the duodenum and the jejunum (Figure 7C). We also observed Peyer's patches filled with chyle (Figure 7C). Occasionally, chyle-filled lymphatic vessels were also observed in other internal organs, such as the heart (Supplemental Figure 5E). Mesenteric lymphatic collecting vessels were often surrounded with chyle effusion in *Foxc2*^{lecKO} animals (Figure 7C).

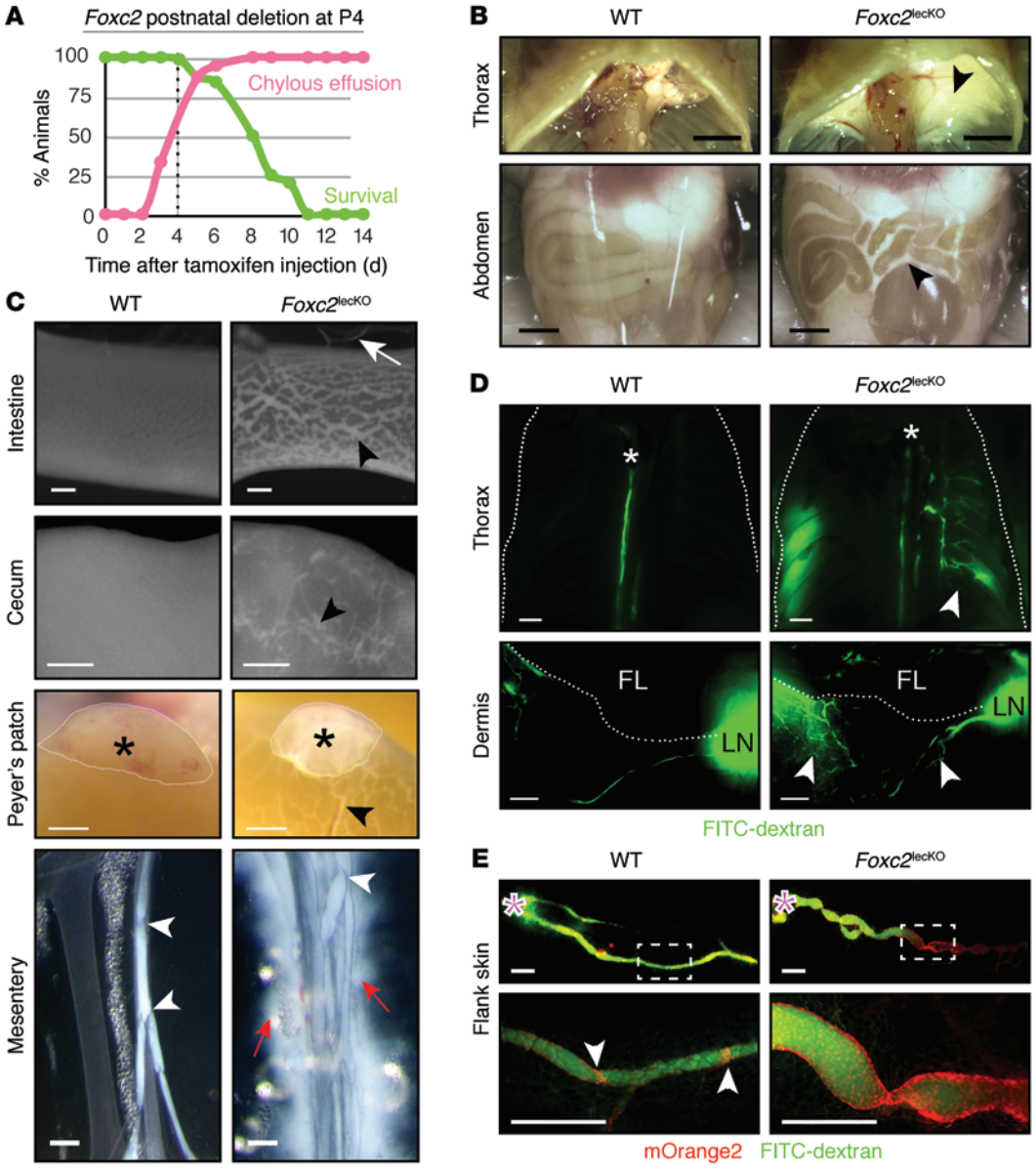

Figure 7. FOXC2 is essential for postnatal lymphatic vascular function. (**A**) Time course of chylous effusion (pink curve) and lethality (green curve) after *Foxc2* inactivation. The dotted line indicates the time point used for most phenotypic analyses. Chylous effusion was defined as the presence of chylothorax or chylous ascites. n = 150 animals (5–20 *Foxc2*^{lecKO} mice per time point). (**B**) Macroscopic appearance of chylothorax (top row) and chylous ascites (bottom row) in P8 *Foxc2*^{lecKO} mice. The arrowheads indicate chyle. (**C**) Chyle accumulation in the intestinal submucosal lymphatic vessels, in the ceca, and in Peyer's patches (asterisk) and chyle leakage from mesenteric lymphatic collecting vessels in P8 *Foxc2*^{lecKO} mice. Black arrowheads indicate chyle accumulation. The white arrow indicates mesenteric vessels. White arrowheads indicate valves. Red arrows indicate chyle leakage. (**D**) Lymph reflux from the thoracic duct and from dermal collecting lymphatic vessels in P8 *Foxc2*^{lecKO} mice. Collecting lymphatic vessels were visualized by FITC-dextran injection into the mesenteric lymph node (top row) or the forelimb foot pad (bottom row). Asterisks indicate thoracic ducts. Arrowheads indicate backflow into lymphatic branches. FL, forelimb; LN, axillary lymph node. (**E**) Impaired lymph transport in *Foxc2*^{lecKO} *Prox1*-mOrange2^{+} pups at P8. FITC-dextran was injected into the inguinal lymph node (asterisks) and visualized in the dermal efferent collecting vessel. *Foxc2*^{lecKO} animals often showed arrest of the lymph drainage at the site of a misshapen valve with lumen narrowing. Arrowheads indicate valves (see also Supplemental Figure 5). Scale bars: 2 mm (**B**); 250 μm (**C**); 1 mm (**D**); 500 μm (**E**).

These data suggested a highly abnormal lymph transport in *Foxc2*^{lecKO} mice. To analyze the lymphatic drainage, we injected fluorescent FITC-dextran into the mesenteric lymph nodes of control or *Foxc2*^{lecKO} mice. As expected, we observed filling of the thoracic ducts in control mice (Figure 7D). In contrast, *Foxc2*^{lecKO} mice had dye outflow in multiple afferent collecting lymphatic vessel branches, indicating lymph backflow. This observation was confirmed by dye injection into the foot pads or the inguinal lymph nodes (Figure 7, D and E). Of interest, *Foxc2*^{lecKO} collecting lymphatic vessels were abnormally patterned, with alternating areas of vessel ectasia and constrictions (Figure 7E).

Taken together, these data demonstrate that the continuous expression of FOXC2 is required for postnatal lymphatic vascular function.

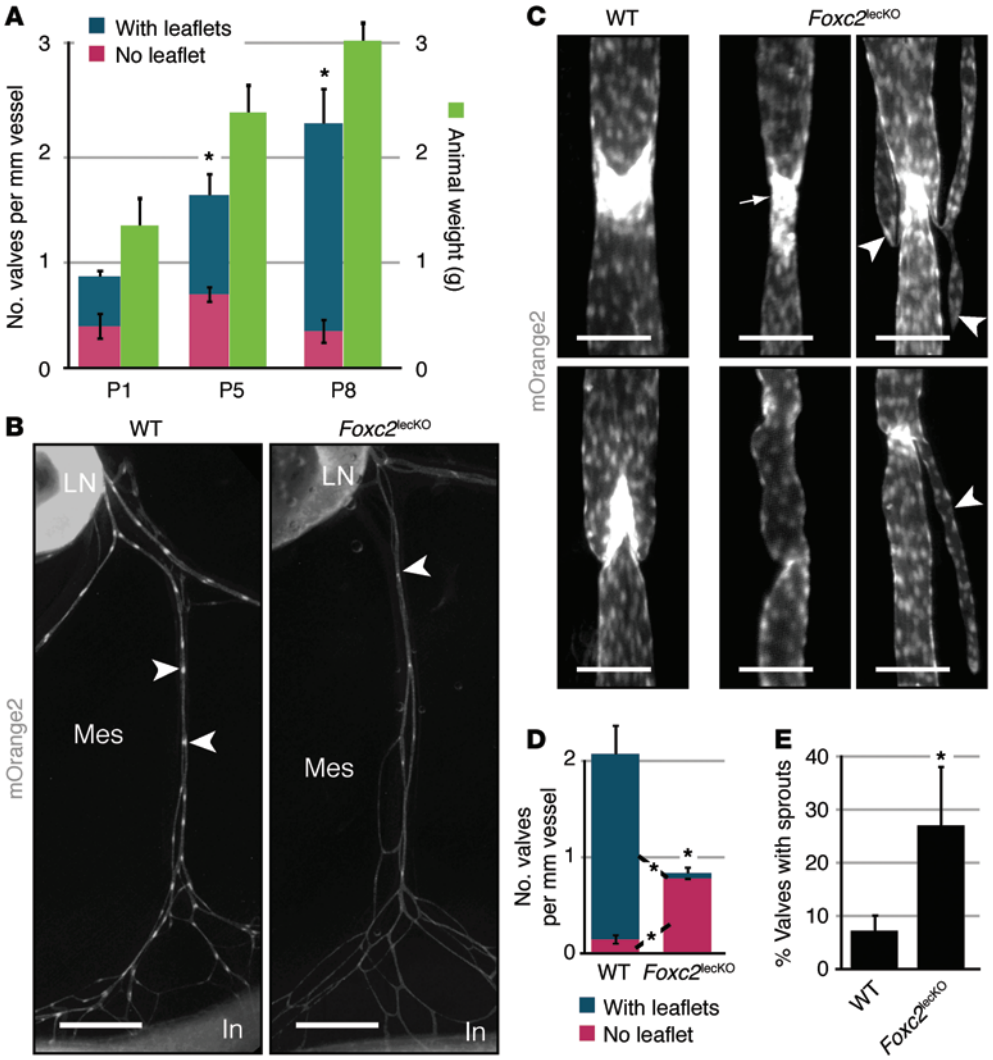

Figure 8. Maintenance of postnatal lymphatic valves depends on FOXC2. (**A**) Time course of postnatal development and maturation of mesenteric lymphatic valves in *Prox1*-mOrange2$^+$ wild-type animals. The total valves per mesentery was 285 ± 24 at P1, 528 ± 90 at P5, and 756 ± 99 at P8. (**B**–**E**) Mice were injected with tamoxifen at P4 and analyzed at P8. (**B**) Organization of mesenteric lymphatic vasculature in P8 mOrange2$^+$ control and *Foxc2*^{lecKO} mice. Arrowheads indicate valves. LN, lymph node; Mes, mesentery; In, intestine. (**C**) High-magnification images of lymphatic valves shown in **B**. Wild-type valves have a semilunar (top row) or a v-like shape (bottom row), depending on their orientation. *Foxc2*^{lecKO} valves are disorganized and misshapen. The arrow indicates a regressing valve. Arrowheads indicate sprouts from the valve site. (**D**) Quantification of the valve number and valve leaflet status. (**E**) Quantification of sprouts associated with *Foxc2*^{lecKO} lymphatic valves, as shown in **C**. n = 4–6; 4 vessels were scored per mesentery; 2-tailed unpaired Student's t test; $^*P < 0.05$. Scale bars: 1 mm (**B**); 50 μm (**C**).

FOXC2 maintains the postnatal collecting lymphatic vessel phenotype. We next crossed the *Foxc2*^{lecKO} line with the *Prox1*-mOrange2 reporter strain, which allows better detection of LECs through the expression of a fluorescent transgene (refs. 10, 23, and Supplemental Figure 5B). In particular, lymphatic valves can be clearly identified, due to high levels of *Prox1* expression in the leaflets.

Quantification demonstrated that numerous valves were already present in mesenteric lymphatic vessels at birth and that their number continued to increase during postnatal development, in line with the continuous animal growth at this stage (Figure 8A). Control mesenteries at P8 showed well-developed collecting lymphatic vessels, characterized by even lymphangion diameter, and up to 800 valves positioned at regular intervals along the mesenteric vessels (Figure 8, A and B). Inactivation of *Foxc2* induced degeneration of the lymphatic valves, leading to a significant decrease both in the total number of valves and in the proportion of fully formed valves containing 2 intraluminal leaflets (Figure 8, B–D). The number of valves in *Foxc2*^{lecKO} mice was lower than that at the beginning of tamoxifen administration, demonstrating that *Foxc2* inactivation affects both growing and established lymphatic valves (Figure 8D). A similar phenotype was observed when using the *Flt4*-Cre^{ERT2} deleter strain to inactivate *Foxc2* in the lymphatic endothelium (Supplemental Figure 6, A–C).

The spectrum of lymphatic valve defects in *Foxc2*^{lecKO} mice ranged from shortened leaflets to an almost complete absence of PROX1^{hi} valve cells (Figure 8C), with vessel constriction often being the only sign of the former valve location. As *Foxc2* deletion in lymphatic valves was nearly complete (Supplemental Figure 5D), the variability in the severity of valve defects may be related to local conditions, such as changes in flow. Fluorescent microlymphangiography demonstrated greatly reduced or absent flow through stenotic valve areas, suggesting vessel lumen obstruction (Figure 7E). Surprisingly, in a significant proportion of *Foxc2*^{lecKO} vessels, we observed the formation of ectopic sprouts extending from the degenerating lymphatic valve sinuses and growing in the direction opposite to the normal lymph flow (Figure 8, C and E). In some cases, such ectopic sprouts further reconnected to the main lymphatic vessel, likely providing an alternative drainage route from the obstructed area.

Foxc2 deletion in older pups (Supplemental Figure 7, A and B) or in adult mice (Figure 9A) also led to lymphatic valve degeneration. In adult mice, we observed significantly impaired lymphatic valve function, as determined by measuring the pressure required to close the valves in isolated mesenteric lymphatic vessels (Figure 9B and Supplemental Figure 7, C–F). As expected, valves in

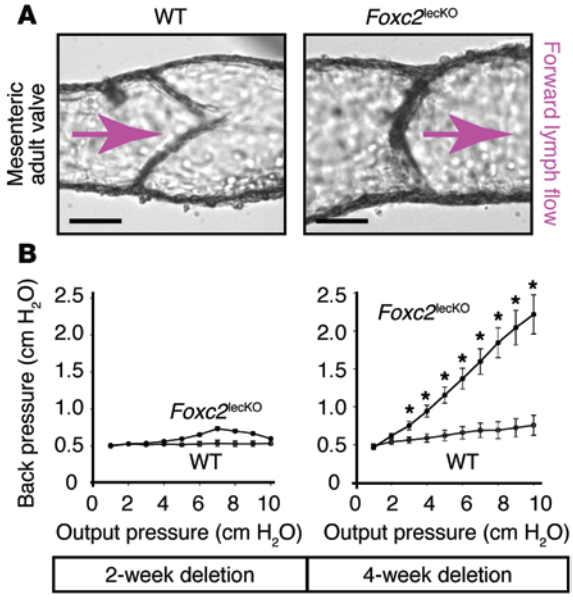

Figure 9. Characterization of functional defects in adult *Foxc2*^{lecKO} valves. (**A**) Examples of wild-type and *Foxc2*^{lecKO} valves from 8-week-old mice treated with tamoxifen for 4 weeks. Equal pressure was applied on both cannulated ends (P_{in}/P_{out}) to open the valve. Arrows indicate forward lymph flow direction. (**B**) Decreased resistance of *Foxc2*^{lecKO} valves. Low pressure back-leak tests of mesenteric valves isolated from mice after 2 or 4 weeks of *Foxc2* inactivation (see also Supplemental Figure 7). n = 5 mice per group; 4–16 valves were scored per condition; 1-way ANOVA with Tukey-Kramer post-hoc test; *$P < 0.05$. Scale bars: 40 μm.

Foxc2^{lecKO} adult mice displayed reduced resistance to increasing backflow pressures and leakiness (Figure 9B and Supplemental Figure 7, E and F) due to leaflet regression (Figure 9A).

Intraluminal valves, smooth muscle cell coverage, and lack of expression of lymphatic capillary markers, such as LYVE-1, are distinguishing features of collecting lymphatic vessels (6, 7). Lymphatic valve endothelial cells produce high levels of specialized extracellular matrix proteins, such as laminin α5 (24). Valve degeneration in *Foxc2*^{lecKO} animals was associated with disruption and detachment of the laminin α5^{+} valve matrix (Figure 10A). Overall, smooth muscle cell recruitment to lymphangions was not significantly affected in *Foxc2*^{lecKO} mice; in contrast, areas of degenerating valves were frequently covered with mural cells, while they were sparse in the valve areas of control mice (Figure 10B). Consistent with previous reports, LYVE-1 was virtually absent from the collecting vessels of wild-type mice (refs. 6, 9, 25, and Figure 10C). However, we observed widespread ectopic reexpression of LYVE-1 in the mesenteric lymphatic vessels of *Foxc2*^{lecKO} mice (Figure 10, C and D).

Taken together, these data demonstrate that FOXC2 is necessary for postnatal development and maintenance of key characteristics of the collecting vessels, such as intraluminal valves, patterning of vascular smooth muscle cells, and appropriate vascular lumen size (Figure 10E).

FOXC2 controls cell shape and cell-cell junctions in vivo. Loss of valves in *Foxc2*^{lecKO} mice demonstrates a critical role for FOXC2 not only in postnatal lymphatic valve development, but also in maintenance. It also raises the question of whether regression of valve leaflets is sufficient to explain the lethal phenotype of *Foxc2*^{lecKO} mice. Gap junction protein connexin37 (CX37) is regulated by FOXC2 during embryonic development, and *Cx37*$^{-/-}$ mice have severe impairment of lymphatic valve formation and lymph backflow (10, 26). However, *Cx37*$^{-/-}$ mice, which lack lymphatic valves to the same extent as *Foxc2*^{lecKO} animals, did not develop chylous ascites or chylothorax and survived normally into adulthood (Supplemental Figure 8, A and B, and data not shown). Thus, while valve degeneration explains lymph backflow (Figure 7D), it is not sufficient to account for chyle leakage and for the generalized collecting lymphatic vessel dysfunction observed in *Foxc2*^{lecKO} mice.

Endothelial cells in lymphatic capillaries have discontinuous cell-cell junctions, which are important for the unimpeded uptake of interstitial fluid. In contrast, endothelial cells in collecting vessels are connected by continuous "zipper-like" junctions, which minimize the loss of lymph during its transport (27). Junction disruption in *FOXC2*^{KD} cells in vitro and increased lymph leakage in *Foxc2*^{lecKO} mice suggest a loss of vascular barrier integrity (Figure 4 and Figure 7C). Therefore, we investigated the state of endothelial junctions by staining collecting lymphatic vessels for VE-cadherin. Endothelial cells in collecting vessels of wild-type mice were elongated in the direction of lymph flow and displayed continuous linear cell-cell junctions with high levels of VE-cadherin (Figure 11, A and B). However, only 3 days after *Foxc2* inactivation, cells already had a more rounded shape (Figure 11, A and B). Most importantly, continuous linear cell-cell junctions were replaced by distinct zigzag-like junctions (Figure 11, B and C). At later stages, reduced and punctuated VE-cadherin staining was observed, demonstrating a disruption of intercellular junctions (Supplemental Figure 9A). This was in agreement with our in vitro observation of intercellular gaps formed in *FOXC2*^{KD} cells under oscillatory and, to a lesser extent, laminar shear stress (Figure 4, B and F, and Supplemental Figure 9B). In addition, endothelial junction protein claudin5, which is highly expressed in wild-type collecting vessels, was also reduced in *Foxc2*^{lecKO} degenerating valve areas (Supplemental Figure 9C).

We further examined the morphology of endothelial cell-cell junctions in the thoracic duct using transmission electron microscopy. In wild-type mice, endothelial cells formed a thin and continuous monolayer surrounded by a thick and dense basement membrane (Figure 11D). However, in *Foxc2*^{lecKO} animals, the endothelium appeared disrupted in several sites and associated with a loose and disorganized extracellular matrix, indicative of increased endothelial permeability (Figure 11D). Surprisingly, disruption of the endothelium was characterized by the formation of large vacuole-like structures, which formed thin sheet-like fragments shedding into the lumen (Figure 11D). Further examination of cell-cell contacts revealed that wild-type endothelial cells had well-organized interdigitating contacts tightly bound to the matrix (Figure 11, E–G). However, the majority of such contacts in *Foxc2*^{lecKO} cells were unfolded, resulting in the formation of large vacuoles and endothelial cell detachment from the matrix below (Figure 11, D–G), indicating severe loss of intercellular junction integrity.

Thus, we propose that loss of junction integrity in the absence of FOXC2 is responsible for lymph leakage and development of chylous effusion (Figure 10E). In addition, such vessels may be

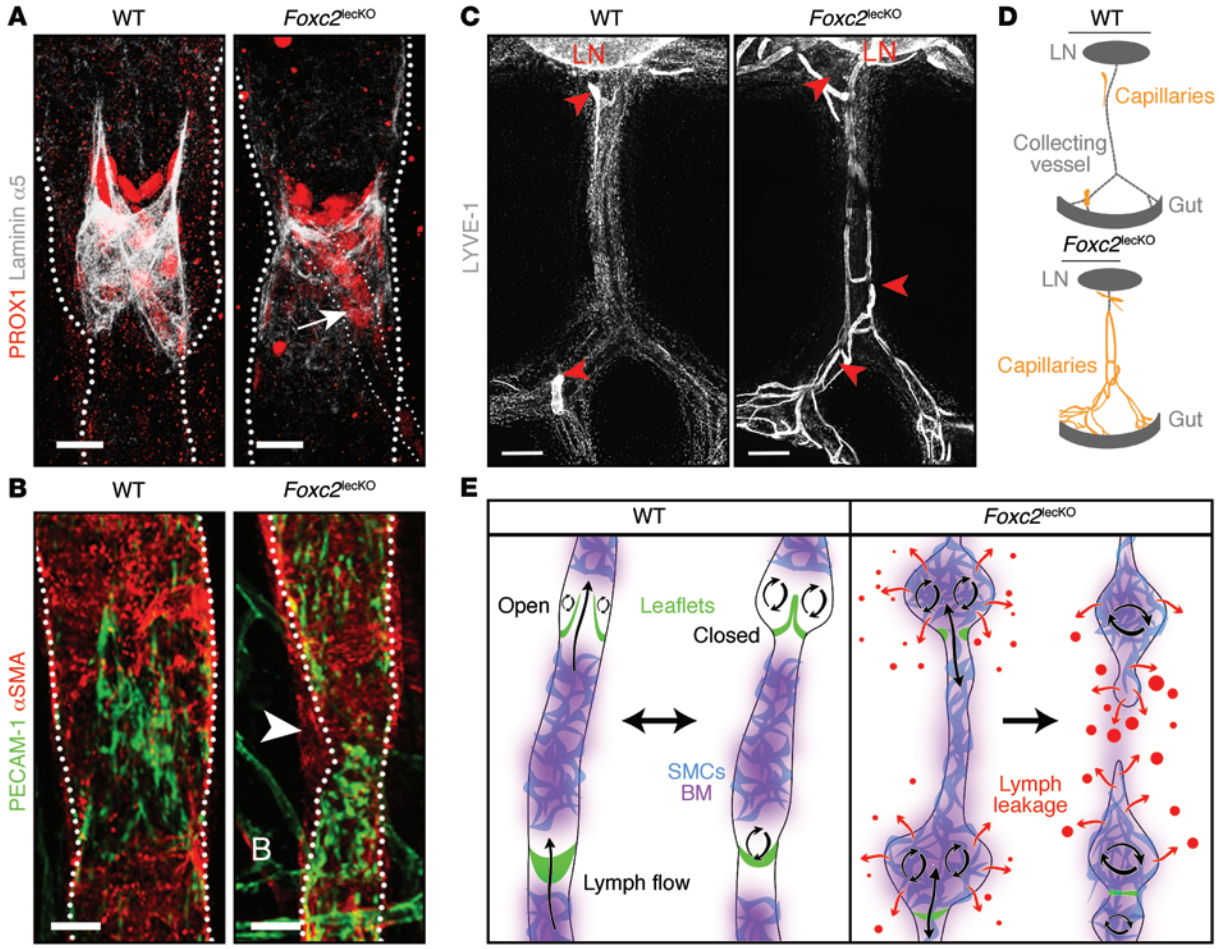

Figure 10. FOXC2 maintains collecting lymphatic vessel phenotype. (**A**) Reduced valve core matrix in mesenteric lymphatic vessels of *Foxc2*^{lecKO} P8 mice. Staining for laminin α5 (white) and PROX1 (red). The collecting vessel is outlined with dashed white lines. The arrow indicates sprout from the valve sinus. (**B**) Vascular smooth muscle cell coverage on mesenteric lymphatic valves of *Foxc2*^{lecKO} P8 mice (arrowhead). Staining for αSMA (red) and PECAM1 (green). The collecting vessel is outlined with dashed white lines. B, blood vessel. (**C**) Increased levels of LYVE-1 (white) in collecting mesenteric lymphatic vessels of P8 *Foxc2*^{lecKO} mice. Arrowheads indicate LYVE-1$^+$ vessels. Some immune cells are also LYVE-1$^+$ along the vascular branches. LN, lymph node. (**D**) Scheme recapitulating LYVE-1 staining shown in **C**. (**E**) *Foxc2*^{lecKO} collecting vessels display valve regression, lumen collapse, and increased lymph leakage. Extreme narrowing of the vessel in the degenerating valve area could eventually lead to vessel rupture, precipitating accumulation of the lymph (e.g., in the pleural cavity). Scale bars: 20 μm (**A** and **B**); 500 μm (**C**).

less resistant to increased luminal pressure, stretch, and disturbed flow, all of which are prominent in valve sinuses (11). As a consequence, *Foxc2*^{lecKO} collecting vessels may become extremely fragile at sites of degenerating valves and lumen obstruction (Figure 7E), which may lead to vessel rupture and catastrophic lymph leakage or alternatively to compensatory collateral lymphatic vessel sprouting from obstructed valve sites (Figure 8C).

FOXC2 controls cell quiescence and survival in vivo. We next sought to investigate the cellular mechanisms implicated in valve regression and lumen collapse at the former valve site. The number of PROX1^{hi} valve cells was reduced in *Foxc2*^{lecKO} vessels already 2.5 days after tamoxifen administration (Supplemental Figure 10A and Supplemental Video 9). We examined LEC apoptosis in control and *Foxc2*^{lecKO} mice by staining for activated caspase-3 and PROX1. While apoptosis was barely detectable in wild-type samples, a significant number of apoptotic cells were observed in the valves of *Foxc2*^{lecKO} vessels (Figure 12, A and B). A careful examination revealed that *Foxc2*^{lecKO} apoptotic cells were often arranged in doublets with symmetrically organized PROX1^{hi} apoptotic bodies (Figure 12, C and D), indicating that apoptosis might occur in dividing cells. To address this question, we stained wild-type and *Foxc2*^{lecKO} mesenteries for PROX1 and the cell proliferation marker Ki67 to identify proliferating LECs that undergo cell death. Surprisingly, but in line with our in vitro results, a markedly higher proportion of PROX1$^+$/Ki67$^+$ cells was found in *Foxc2*^{lecKO} collecting vessels compared with that in control collecting vessels (Figure 12E), demonstrating increased cell proliferation. Interestingly, 78.7% ± 13.7% of the *Foxc2*^{lecKO} valves (n = 3 animals) showed at least one cell death event, which was characterized by PROX1$^+$ apoptotic bodies (Figure 12F and ref. 28). Half of the *Foxc2*^{lecKO} dying cells (50.6% ± 27.9%, n = 3 animals; Figure 12G) were double positive for PROX1 and Ki67, further reinforcing the link between cell proliferation and death in *Foxc2*^{lecKO} vessels. In contrast, we were unable to detect double-positive PROX1/Ki67 dying cells in the wild-type samples. We further validated the increased LEC proliferation in *Foxc2*^{lecKO} vessels, using the EdU incorporation assay to detect DNA synthesis (Figure 13, A and B). A significantly higher proportion of proliferating LECs

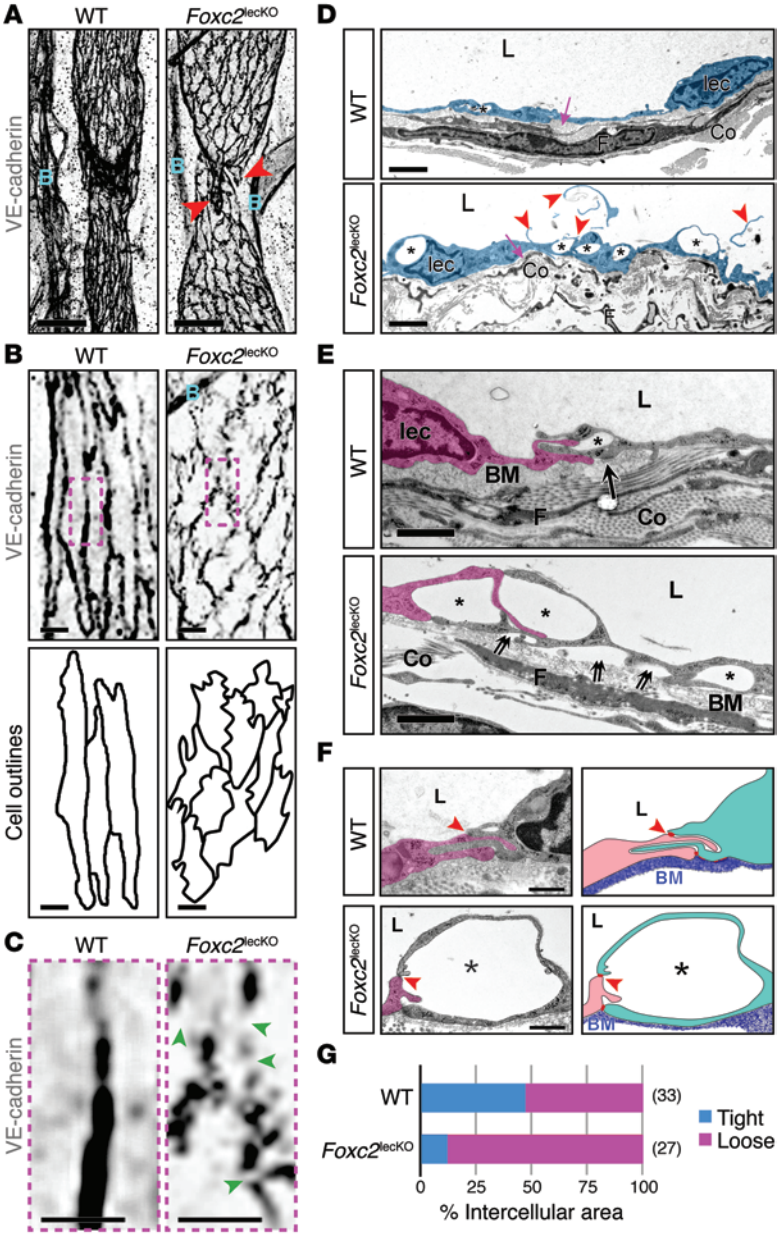

Figure 11. FOXC2 controls cell-cell junction integrity in collecting vessels. (**A**) Impaired cell elongation in *Foxc2*^{lecKO} P7 mesenteric collecting lymphatic vessels. Staining for VE-cadherin. Red arrowheads indicate lymphatic sprouts from valve sinuses. B, blood vessels. (**B**) Continuous VE-cadherin pattern in wild-type LECs and zigzag-like junctions in *Foxc2*^{lecKO} LECs. The bottom row shows outline of the cells. B, blood capillary. (**C**) High-magnification images of the junctions from the pink boxed area in **B**. *Foxc2*^{lecKO} junctions have multiple gaps (green arrowheads). (**D**) Transmission electron microscopy images of P8 wild-type and *Foxc2*^{lecKO} thoracic duct transverse sections. L, lymphatic lumen; F, fibroblast; lec, endothelial nucleus; Co, collagen fibers. Asterisks indicate endothelial vacuoles; red arrowheads indicate sheet-like structures shedding into the lumen; pink arrows indicate basement membrane. The lymphatic endothelium is highlighted in blue. (**E** and **F**) Transmission electron microscopy images of LEC junctions in the thoracic duct. Neighboring cells (the left one is pseudo-colored in pink) have "interdigitating" contacts, fixed on both ends by junctional complexes (red arrowheads in **F**) and to the basement membrane (BM) via adhesion complexes (arrows). *Foxc2*^{lecKO} cell-cell contacts are unfolded, resulting in the formation of interendothelial vacuoles (asterisks), which often detach from the matrix below (double arrows). Co; collagen fibers; L, vessel lumen. A scheme of the intercellular junctions shown on the left in **F** is provided on the right. (**G**) Quantification of endothelial cell-cell junction organization in the thoracic ducts of *Foxc2*^{lecKO} and control mice. Percentage of tight (see wild-type junction in **F**) or loose (see *Foxc2*^{lecKO} junction in **F**) cell-cell junctions is shown for each genotype together with the number of junctions analyzed (see also Supplemental Figure 9). Scale bars: 50 μm (**A**); 10 μm (**B** and **C**); 2 μm (**D**); 1 μm (**E**); 250 nm (**F**).

was found in *Foxc2*^{lecKO} collecting vessels compared with that in control collecting vessels (Figure 13C), while lymphatic capillaries of both control and *Foxc2*^{lecKO} mice displayed comparable proliferation rates (Supplemental Figure 10B).

Our in vitro experiments suggested that enhanced proliferation in the absence of FOXC2 is mediated by the increased activity of the Hippo pathway effector TAZ (Figure 6). Moreover, we observed TAZ nuclear localization in the lymphatic collecting vessels, particularly in valves (Figure 6D) and in Ki67^{+} LECs in *Foxc2*^{lecKO} mice (Supplemental Figure 10C). To study TAZ activity in vivo, we isolated lymphangion and lymphatic valve endothelial cells from the mesenteric vessels of wild-type or *Foxc2*^{lecKO} *Prox1*-mOrange2 animals using FACS (Supplemental Figure 10D). As expected, valve cells expressed higher levels of the *mOrange2* transgene and valve markers *Prox1*, integrin α9, and *Cx37* in comparison to lymphangion cells (Figure 13, D and E, and Supplemental Figure 10E). *Cx37* levels were decreased in *Foxc2*^{lecKO} cells, in line with previously published results (Figure 13E, Supplemental Figure 10E, and refs. 10, 26). Most importantly, FOXC2-deficient valve LECs expressed higher levels of the YAP1/TAZ targets *Ctgf*, *Cyr61*, and *Ankrd1*, further supporting the notion that FOXC2 restricts TAZ activity in vivo (Figure 13F and Supplemental Figure 10E).

Collectively, these experiments suggest that FOXC2 is important for the maintenance of collecting vessel endothelial cell quiescence and survival. In the absence of FOXC2, LECs undergo TAZ-dependent inappropriate proliferation, which is also accompanied by increased apoptosis, resulting in valve cell loss and vessel lumen narrowing.

Inactivation of FOXC2 only in the valve areas recapitulates the postnatal lethality phenotype. Our in vitro data indicate that a combination of FOXC2 loss of function and increased mechanical strain, such as OSS, is necessary to disrupt cell-cell junctions and to

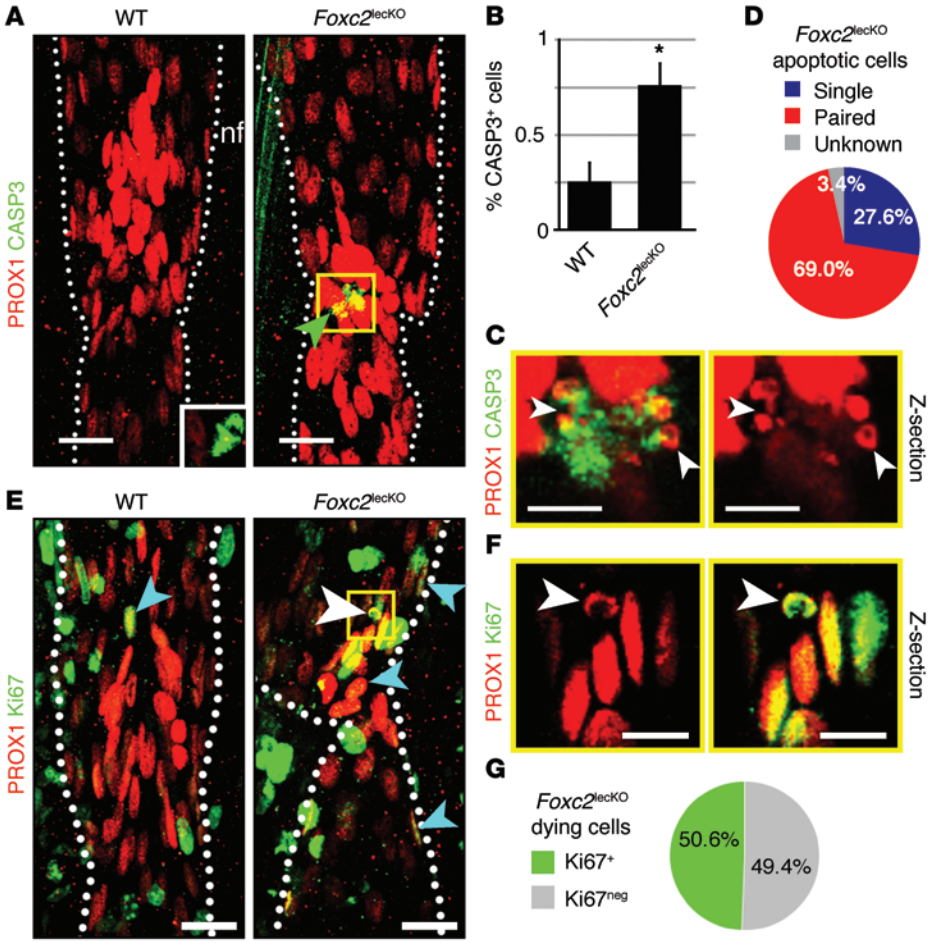

Figure 12. FOXC2 maintains cell quiescence and survival in vivo. (**A**) Increased apoptosis in *Foxc2*^{lecKO} lymphatic collecting vessels 2 days after *Foxc2* inactivation. Staining for PROX1 (red) and activated caspase-3 (green). Only rare CASP3$^+$ nonendothelial cells were observed in the wild-type samples (inset). Dotted white lines outline the collecting vessel. (**B**) Quantification of PROX1$^+$/CASP3$^+$ cells. n = 3–5; 5–10 valves scored per mesentery; 2-tailed unpaired Student's t test; $^*P < 0.005$. (**C**) High-magnification images of the area outlined by the yellow box in **A**. *Foxc2*^{lecKO} apoptotic cells were often arranged in doublets with PROX1^{hi} symmetrically organized apoptotic bodies (white arrowheads). (**D**) Proportion of PROX1$^+$/CASP3$^+$ apoptotic cell doublets (blue) or singlets (red) in *Foxc2*^{lecKO} mesenteries. WT, n = 2 animals; *Foxc2*^{lecKO}, n = 4 animals. (**E**) Increased LEC proliferation in *Foxc2*^{lecKO} collecting vessels. Staining for Ki67 (green) and PROX1 (red) 3 days after *Foxc2* inactivation. Dotted white lines outline collecting vessels. Blue arrowheads indicate PROX1$^+$/Ki67$^+$ cells. (**F**) High-magnification image of a dying LEC with a fragmented PROX1$^+$/Ki67$^+$ pattern (white arrowhead) from the area outlined by the yellow box in **E**. (**G**) Proportion of the PROX1$^+$/Ki67$^+$ double-positive apoptotic cells in *Foxc2*^{lecKO} mesenteries. No PROX1$^+$/Ki67$^+$ apoptotic bodies were observed in wild-type mesenteries. n = 3 mice per genotype. Scale bars: 20 μm (**A** and **E**); 10 μm (**C** and **F**).

initiate abnormal cell proliferation and death, which would impair lymphatic vascular function in vivo. Therefore, inactivation of *Foxc2* only in areas of disturbed flow, such as valves, should recapitulate the lethal phenotype observed in mice with inactivation of *Foxc2* in all LECs. To test this hypothesis, we generated *Foxc2*$^{fl/fl}$ *Prox1*-Cre^{ERT2} *Rosa26*-YFP and *Prox1*-Cre^{ERT2} *Rosa26*-YFP mice, in which administration of tamoxifen genetically marks recombined cells with YFP. We next titrated the dosage of tamoxifen to 3 μg/g to achieve a mosaic deletion of *Foxc2* in P4 mice. At this concentration, recombination was observed only in 5% to 10% of cells, preferentially in the valve areas, likely due to higher *Prox1* promoter activity (Figure 14A). We quantified the number of YFP$^+$ cells in the lymphatic vessels of control and *Foxc2*^{lecKO} animals 2 days after tamoxifen injection, which was prior to the appearance of valve structure defects. There was a significant decrease in the number of YFP$^+$ cells in *Foxc2*^{lecKO} valves compared with that in wild-type valves, while YFP expression was comparable in other PROX1-expressing tissues, such as eye lenses, in the control and *Foxc2*^{lecKO} mice (Figure 14 and data not shown). These data are in line with the observed increased apoptosis (Figure 12, A and B), and they confirm that *Foxc2*-deficient cells were rapidly eliminated from valve regions. Most importantly, such localized inactivation of FOXC2 resulted in the development of chylothorax and fully penetrant animal lethality (0 of 7 *Foxc2*^{lecKO} mice vs. 6 of 6 control mice were alive 2 weeks after tamoxifen injection), thus recapitulating the defect of lymphatic vessels with complete inactivation of *Foxc2*. As a marked proportion of the PROX1^{hi} leaflet cells was in direct contact with the PROX1^{lo} lymphangion cells (Supplemental Figure 11), junctional defects and the abnormal proliferation/apoptosis rate of such FOXC2-deficient PROX1^{hi} cells likely lead not only to valve leaflet regression, but also to vessel wall disruption, lymph leakage, and subsequent mouse death. We therefore propose that lymphatic valve areas represent critically vulnerable regions in collecting lymphatic vessels, which require especially high levels of FOXC2 to ensure vessel integrity and normal function of the entire lymphatic vessel network.

Discussion

Quiescence, barrier integrity, and functional specialization are key properties of the postnatal vasculature. At present, little is known about the regulation of these traits in lymphatic vessels, despite increasing understanding of their importance in both normal physiology and many diseases, such as cancer, inflammation, obesity, hypertension, and atherosclerosis (4, 5). Our ability to therapeutically modulate lymphatic vascular function — and thus potentially treat some of the major diseases — needs better understanding of the molecular processes important for lymphatic vascular stabilization, specialization, and maintenance. Here, we report that function of postnatal collecting lymphatic vessels critically depends on the transcription factor FOXC2.

By using an inducible loss-of-function genetic mouse model, we show that, in the absence of FOXC2, there is a rapid loss of collecting lymphatic vessel specialization and function. Such

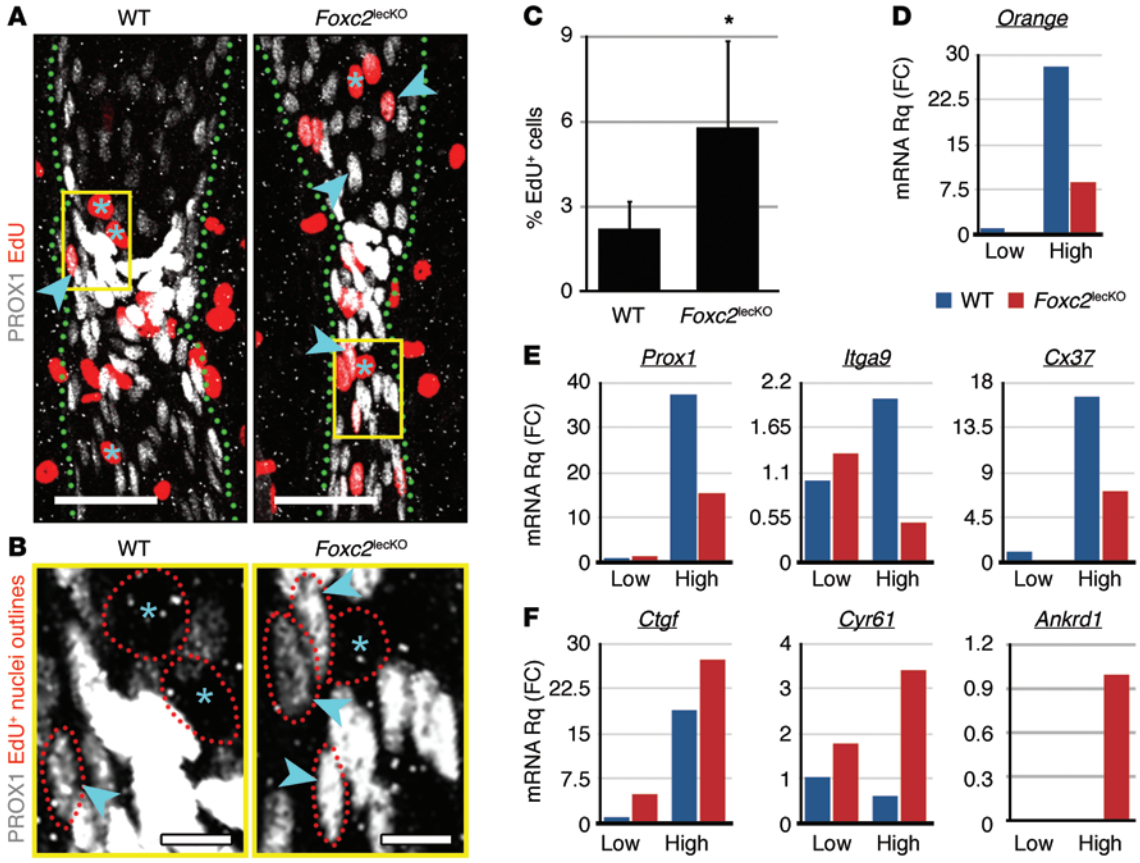

Figure 13. FOXC2 promotes cell growth arrest and counteracts TAZ signaling. (**A**) Increased proliferation in *Foxc2*^{lecKO} lymphatic collecting vessels. DNA synthesis was detected by EdU incorporation 2 days after tamoxifen injection. Staining for PROX1 (white) and EdU (red). Dotted green lines outline the collecting vessel. (**B**) High-magnification images of the area in the yellow box from **A** (PROX1 staining only). The dashed red lines outline the EdU$^+$ nuclei. Blue arrowheads indicate EdU$^+$/PROX1$^+$ nuclei; blue asterisks indicate EdU$^+$/PROX1$^-$ nuclei. (**C**) Quantification of EdU$^+$/PROX1$^+$ cells in the collecting vessels of control or *Foxc2*^{lecKO} mice. n = 9; 5 valves scored per mesentery; 2-tailed unpaired Student's t test; $^*P < 0.01$. (**D**) Orange transgene expression levels in mesenteric lymphangion (Orange^{lo}) and valve cells (Orange^{hi}) isolated from *Prox1*-mOrange2$^+$ and *Foxc2*^{lecKO} *Prox1*-mOrange2$^+$ pups 2 days after tamoxifen injection. (**E**) Valve markers *Prox1*, *Itga9*, and *Cx37* are elevated in Orange^{hi} control LECs. *Cx37* is reduced in *Foxc2*-deficient LECs, as reported previously (10, 26). (**F**) Enhanced expression of TAZ target genes *Ctgf*, *Cyr61*, and *Ankrd1* in LECs of *Foxc2*^{lecKO} mice. Data are representative of 2 independent experiments. The second experiment is shown in Supplemental Figure 10E (see also Supplemental Figure 10 and Supplemental Video 9). Scale bars: 50 μm (**A**); 100 μm (**B**).

changes are characterized by degeneration of the lymphatic valves, decreased vascular barrier properties, ectopic endothelial proliferation and apoptosis, and loss of a patent vascular lumen at the sites of former valves (Figure 15). FOXC2 is highly expressed in the lymphatic valve sinuses, which are constantly solicited by complex fluid flow patterns and mechanical stretch, due to valve opening and closure (Figure 15). In addition, the valve site lacks smooth muscle cells, which normally provide prosurvival and stabilizing signals to the vascular endothelium (e.g., Figure 10B). Thus, we propose that continuous high FOXC2 expression is critical for the stability and function of these regions and, ultimately, normal function of the entire lymphatic vascular network.

We have shown previously that FOXC2 expression is induced by OSS (10). Here, we propose a model for the self-organization and maintenance of lymphatic valve regions in which FOXC2 plays a central role (Figure 15). In such a model, recirculating lymph flow, generated because of the geometry of the valves, induces high expression of FOXC2. FOXC2, in turn, maintains lymphatic valve leaflet and sinus integrity by stabilizing cell-cell junction and promoting quiescence and survival of cells subjected to disturbed flow (Figure 15). Inactivation of *FOXC2* leads to loss of mature intercellular junctions and to actin cytoskeleton reorganization, which, we believe, is the initial defect that propagates lymphatic vascular dysfunction by several mechanisms. First, it impairs the collecting vessel barrier function and promotes lymph leakage, directly accounting for the development of chylous effusion (Figure 7, B and C, and Figure 15). Second, it modifies the responses of LECs to fluid shear stress: while disturbed flow promotes the quiescence of FOXC2$^+$ LECs, in the absence of FOXC2, cells respond by activating TAZ signaling, which is further translated into enhanced cell proliferation followed by cell death (Figure 15). YAP1/TAZ are Hippo signaling effectors that play a key role in regulating organ size and tissue growth as well as in cancer (29, 30). However, the role of YAP1/TAZ in endothelial cells is not well understood. While YAP1 seems to have a dominant pro-proliferative function in most cell types, including HUVECs (31, 32), our analyses surprisingly revealed that, in LECs, TAZ, but not YAP1, is a critical regulator of proliferation in OSS and likely other conditions. Another intriguing observation is the fact that OSS induces not only *FOXC2*^{KD} cell proliferation, but also cell death. Progression through the cell cycle requires highly coordinated changes in actin cytoskel-

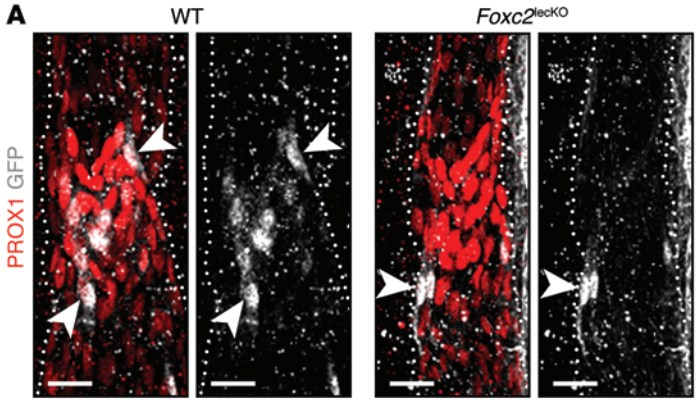

Figure 14. FOXC2 protects valve cells in vivo. (**A**) *Foxc2*^{lecKO} cells are not retained in the valves. Mesenteries from *Rosa26*-YFP WT or *Rosa26*-YFP *Foxc2*^{lecKO} mice were stained for PROX1 (red) and GFP (white) 2 days after *Foxc2* mosaic deletion. Arrowheads indicate PROX1^{+}/YFP^{+} cells. (**B**) Quantification of PROX1^{hi}/GFP^{+} (valve) and PROX1^{lo}/GFP^{+} (lymphangion) cells in wild-type and *Foxc2*^{lecKO} mesenteric vessels (see also Supplemental Figure 11). $n = 3$; 5–10 valves scored per mesentery; 2-tailed unpaired Student's t test; $^{*}P < 0.05$. Scale bars: 25 μm.

eton; therefore, it is possible that the abnormal state of the cytoskeleton in *FOXC2*^{KD} cells, which is especially striking in OSS (Figure 5), interferes with certain steps of cell division and leads to cell death.

In atherosclerosis, disturbed flow increases cell proliferation and apoptosis of blood arterial endothelial cells, leading to the formation of distinct areas with increased expression of proinflammatory genes and vascular permeability, which are thought to initiate the development of atherosclerotic plaques (33). While a side-by-side comparison of responses of different types of BECs and LECs to a range of shear stress values still needs to be carried out, it is of interest that the responses of FOXC2-deficient LECs, such as increased proliferation and cell death, are reminiscent of the BEC behavior in atheroprone regions (2). Lymphatic valves are characterized by disturbed flow, and the mouse mesenteric vessel network contains up to 800 valves. Thus, unlike in blood vessels, areas of low OSS are very common in collecting lymphatic vessels. We therefore postulate that lymphatic vessels evolved a protective mechanism to keep such regions quiescent and functional through the mechanoinduction of FOXC2. In the absence of FOXC2, LECs might revert to the blood endothelial-specific dysfunctional phenotype and therefore be unable to withstand the valve mechanical stress.

FOXC2 is mutated in the human disease of lymphatic vessels, lymphedema-distichiasis, characterized by swelling of the lower limbs and valve defects (8). Since FOXC2 controls a significant part of the mechanoresponses of LECs, it is tempting to suggest that abnormal mechanotransduction is the primary cause of the defects observed in patients with lymphedema-distichiasis. Although 25% of *Foxc2*$^{+/-}$ mice are reported to develop lymphatic vascular defects (34), such incomplete penetrance complicates testing of potential treatment approaches for lymphedema-distichiasis. The rapid and fully penetrant onset of lymphatic vascular dysfunction in our model makes it especially suitable for therapeutic preclinical studies, such as screening of pharmacological agents.

In summary, our work reveals a key role of FOXC2 in the stabilization of collecting lymphatic vessels and maintenance of their function. It establishes a general principle of postnatal lymphatic vascular organization, in which the FOXC2 transcriptional network orchestrates collecting lymphatic vessel phenotype, quiescence, and integrity, through the coordination of cell-cell junction maturation and shear stress responses in the regions of disturbed flow, such as valves. It also uncovers a novel crosstalk between FOXC2 and TAZ in the regulation of LEC quiescence and proliferation. Finally, our work also reveals unexpected differences in the responses to the same mechanical stimuli by blood and LEC lineages. In addition, we suggest that further understanding of how lymphatic vessels avoid deleterious effects of disturbed fluid flow may provide useful information for the prevention or treatment of atherosclerosis.

Methods

Animal models. Generation of *Foxc2*$^{fl/fl}$ mice is described in Supplemental Figure 5A. *Prox1*-Cre^{ERT2}, *Flt4*-Cre^{ERT2}, *Prox1*-mOrange2, *Rosa26*-YFP, and *Cx37*$^{-/-}$ mice were described previously (Supplemental Figure 5B and refs. 23, 35–38). All mice were bred to at least the sixth generation on C57BL6/J background. Pups were injected with 125 μg tamoxifen in 50 μl sunflower oil i.p. or subcutaneously (Supplemental Figure 5C). For mosaic deletion, we used 3 μg/g tamoxifen. Adult mice were treated for 2 to 4 weeks, with 2 injections i.p. per week with 50 μg/g tamoxifen. 5 μg/g EdU (Life Technologies) was injected i.p. 3 hours prior to sacrifice.

Microlymphangiography. Anesthetized *Prox1*-mOrange2^{+} mice were injected with 2 μl of 10 mg/ml 4-kDa FITC-dextran (Sigma-Aldrich) into forelimb foot pads or lymph nodes. Lymphatic drainage was observed under a Leica M205FA stereomicroscope, using Leica camera DFC300FXR2 and LAS AF6000 software.

Mouse tissue collection, staining procedures, and image acquisition. See the Supplemental Methods for detailed information. Supplemental Table 2 lists primary and secondary antibodies and dyes used in the study. All whole-mount staining images are shown with the same orientation, i.e., with the direction of flow from the bottom.

Adult valve back-leak test. Mesenteric lymphatic collecting vessel segments containing one valve were dissected from 8-week-old mice and analyzed as previously described (39, 40). A diagram of the preparation is shown in Supplemental Figure 7C. Briefly, output pressure (downstream) was elevated while monitoring pressure and diameter on the input (upstream) side of the valve (Supplemental Figure 7D). Two tests were performed at low (0.5–10 cm H_2O at a rate of 4 cm H_2O/min) or high (10–60 cm H_2O with each step lasting for 30 seconds) pressure levels.

Transmission electron microscopy. Transmission electron microscopy was performed as previously described (41). Briefly, tissues were immersion fixed in 2.5% glutaraldehyde in PBS, post-fixed in osmium tetroxide, dehydrated in ethanol series, and embedded in epoxy resin. Ultrathin 90-nm sections were mounted on copper grids coated with Formvar (polyvinyl formal; Fluka), stained with lead citrate and uranyl acetate, and analyzed using a Philips EM 400 electron microscope.

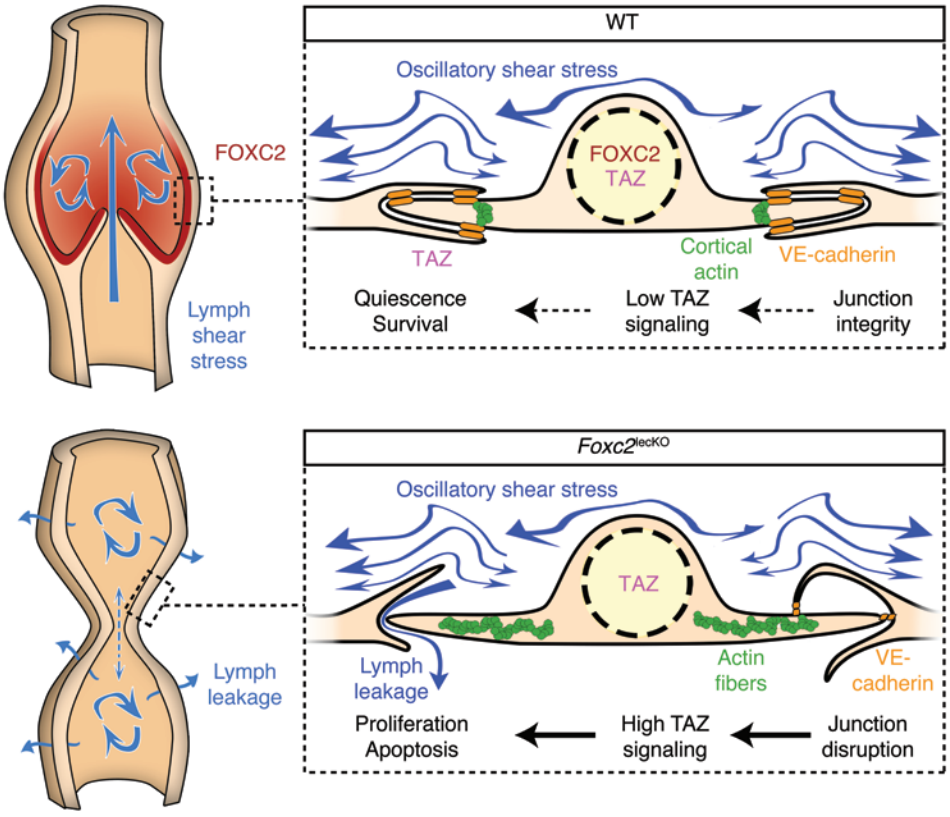

Figure 15. FOXC2 and fluid shear stress stabilize postnatal lymphatic vasculature by enhancing cell-cell junction integrity and inducing cell-cycle arrest. Collecting lymphatic vessels contain a large number of lymphatic valves, characterized by areas of persistent disturbed flow in valve sinuses. Disturbed flow (modeled by OSS) induces expression of FOXC2, formation of overlapping intercellular junctions, and nuclear accumulation of TAZ. FOXC2 protects integrity of the overlapping cell-cell junctions and the cortically organized actin cytoskeleton and prevents the proliferative action of TAZ. In the absence of FOXC2, OSS potentiates the cell-cell junction defects, activates cytoskeleton remodeling, and induces TAZ-dependent cell proliferation and death.

Cell transfection and immunostaining. Human intestinal LECs were cultured as described previously (42). See the Supplemental Methods for detailed information. Supplemental Table 2 lists primary and secondary antibodies and dyes used in the study. siRNAs are listed in Supplemental Table 3. Two different siRNAs or a pool of four were used independently to knockdown the gene of interest. Knockdown efficiency was confirmed for each siRNA by RT-qPCR, Western blot analysis, and/or immunostaining (Figure 3A and Supplemental Figure 1A for *FOXC2*; Supplemental Figure 2B for a second *FOXC2* siRNA; Supplemental Figure 4C for *YAP1*; and Supplemental Figure 4D for *TAZ*).

In vitro flow experiments. LECs were seeded at confluence on fibronectin-coated slides (μ-Slide $I^{0.8}$ Luer; ibidi), cultured for 24 hours, and subjected to oscillatory (4 dynes/cm^2; 0.25 Hz, flow changes direction every 4 seconds) or laminar flow (4 dynes/cm^2) in a parallel plate flow chamber system (ibidi Pump System; ibidi) or kept under static conditions for 48 hours. For full description, see the Supplemental Methods.

Gene expression and bioinformatics analyses. RNA was isolated from FOXC2 or control siRNA-transfected LECs subjected to 24 hours of OSS (1 dyn/cm^2; 0.25 Hz) or kept under static conditions in 2 independent experiments using 2 different *FOXC2* siRNAs. RNA was amplified and hybridized on Affymetrix Human Gene 1.0 ST Arrays, and arrays were scanned and analyzed as described previously (43). The data were corrected for batch effect with the COMBAT method and normalized using Robust Multichip Average (method Bioconductor package affy, R version 3.0.1). Data were submitted to Gene Omnibus Expression (NCBI) under the accession number GSM1466659.

Pathway analyses were performed using R packages String.db and GOstat. The igraph package was used for network layout obtained in String.db. Enrichment for GO (biological process) terms was computed using the conditional hypergeometric test implemented in GOstat. ReviGO was used to summarize GO enrichment lists into groups, and redundant groups were merged into biologically relevant groups by manual curation.

Flow cytometry. P14 mouse mesenteries were digested using Collagenase A (1 mg/ml, Roche)/DNase I (100 μg/ml, Roche) solution with 0.1% BSA. Cell suspension was filtered through a 40-μm cell strainer, washed with 5% FBS in phenol red-free DMEM (Gibco), and sorted on a BD FACSAria III (BD Biosciences) or MoFlo Astrios^{EQ} (Beckman Coulter Life Sciences) cell sorter with BD FACSDiva software (BD Biosciences). Following exclusion of dead cells and multiplets, single mOrange2$^+$ cells were gated using mOrange-PE and PE-TexasRed channels; cells from nontransgenic littermates were used to define the orange gate (Supplemental Figure 10D).

RNA isolation, qPCR, and Western blot analyses. For a full description, see the Supplemental Methods. A list of sequences of PCR primers is provided in Supplemental Table 4.

Quantification. For a full description, see the Supplemental Methods.

Statistics. We used a 2-tailed unpaired Student's *t* test to determine statistical significance by calculating the probability of difference between two means. For valve back-leak test analyses, a custom LabVIEW program (National Instruments) was used to bin the data in 0.1- or 5-cm H2O increments for low- and high-pressure ramps, respectively. The binned data were imported into JMP 8 (SAS Institute) and analyzed using 1-way ANOVAs with Tukey-Kramer post-hoc tests. The differences were considered statistically significant at $P < 0.05$. Data are shown as mean ± SD.

Study approval. Experiments were approved by the Animal Ethics Committee of Vaud, Switzerland, or by the University of Missouri Animal Care and Use Committee.

Acknowledgments

We thank L. Sorokin for laminin α5 antibodies; O. Dormond and J.M. Calmes for help with LEC isolation; C. Beauverd for mouse genotyping, colony maintenance, and help with immunohistochemistry; and S. Piccolo, D. Kerjaschki, G. Halder, and J. Bernier-Latmani for useful discussions. Animal, Cellular Imaging, Flow Cytometry, Genomic Technologies, and Mouse Pathology Facilities of the University of Lausanne are gratefully acknowledged. This work was supported by the Gebert Rüf Foundation, the Swiss National Science Foundation (PPP0033-114898 to T.V. Petrova; CRSII3-141811 to T.V. Petrova, M. Delorenzi, and B.R. Kwak; 31003A_135740 to V. Djonov), La Fondation Leenaards, Theodor and Gabriela Kummer PhD fellowship (to E. Bovay), the People Programme (Marie Curie Actions) of the European Union's Seventh Framework Programme FP7/2007-2013/ under REA grant agreement 317250, the National Institutes of Health (HL-120867 to M.J. Davis), and the Summer Undergraduate Research Programme of University of Lausanne (to E. Gulpinar).

Address correspondence to: Tatiana V. Petrova, Department of Fundamental Oncology, CHUV-UNIL, Ch. des Boveresses 155, CH-1066 Epalinges, Switzerland. Phone: 41.21.314.2968; E-mail: tatiana.petrova@unil.ch.

1. Carmeliet P, Jain RK. Molecular mechanisms and clinical applications of angiogenesis. *Nature*. 2011;473(7347):298–307.
2. Hahn C, Schwartz MA. Mechanotransduction in vascular physiology and atherogenesis. *Nat Rev Mol Cell Biol*. 2009;10(1):53–62.
3. Giannotta M, Trani M, Dejana E. VE-cadherin and endothelial adherens junctions: active guardians of vascular integrity. *Dev Cell*. 2013;26(5):441–454.
4. Coso S, Bovay E, Petrova TV. Pressing the right buttons: signaling in lymphangiogenesis. *Blood*. 2014;123(17):2614–2624.
5. Schulte-Merker S, Sabine A, Petrova TV. Lymphatic vascular morphogenesis in development, physiology, and disease. *J Cell Biol*. 2011;193(4):607–618.
6. Makinen T, et al. PDZ interaction site in ephrinB2 is required for the remodeling of lymphatic vasculature. *Genes Dev*. 2005;19(3):397–410.
7. Petrova TV, et al. Defective valves and abnormal mural cell recruitment underlie lymphatic vascular failure in lymphedema distichiasis. *Nat Med*. 2004;10(9):974–981.
8. Mellor RH, et al. Mutations in FOXC2 in humans (lymphoedema distichiasis syndrome) cause lymphatic dysfunction on dependency. *J Vasc Res*. 2011;48(5):397–407.
9. Norrmen C, et al. FOXC2 controls formation maturation of lymphatic collecting vessels through cooperation with NFATc1. *J Cell Biol*. 2009;185(3):439–457.
10. Sabine A, et al. Mechanotransduction, PROX1, and FOXC2 cooperate to control connexin37 calcineurin during lymphatic-valve formation. *Dev Cell*. 2012;22(2):430–445.
11. Chiu JJ, Chien S. Effects of disturbed flow on vascular endothelium: pathophysiological basis and clinical perspectives. *Physiol Rev*. 2011;91(1):327–387.
12. Kanehisa M, Goto S. KEGG: kyoto encyclopedia of genes and genomes. *Nucleic Acids Res*. 2000;28(1):27–30.
13. Kanehisa M, Goto S, Sato Y, Kawashima M, Furumichi M, Tanabe M. Data, information, knowledge and principle: back to metabolism in KEGG. *Nucleic Acids Res*. 2014;42(Database issue):D199–D205.
14. Dekker RJ, et al. Prolonged fluid shear stress induces a distinct set of endothelial cell genes, most specifically lung Kruppel-like factor (KLF2). *Blood*. 2002;100(5):1689–1698.
15. Gumbiner BM, Kim NG. The Hippo-YAP signaling pathway and contact inhibition of growth. *J Cell Sci*. 2014;127(pt 4):709–717.
16. Petrova TV, et al. Lymphatic endothelial reprogramming of vascular endothelial cells by the Prox-1 homeobox transcription factor. *EMBO J*. 2002;21(17):4593–4599.
17. Fernandez-Martin L, et al. Crosstalk between reticular adherens junctions and platelet endothelial cell adhesion molecule-1 regulates endothelial barrier function. *Arterioscler Thromb Vasc Biol*. 2012;32(8):e90–e102.
18. Huveneers S, et al. Vinculin associates with endothelial VE-cadherin junctions to control force-dependent remodeling. *J Cell Biol*. 2012;196(5):641–652.
19. Schlegelmilch K, et al. Yap1 acts downstream of alpha-catenin to control epidermal proliferation. *Cell*. 2011;144(5):782–795.
20. Zhao B, et al. Angiomotin is a novel Hippo pathway component that inhibits YAP oncoprotein. *Genes Dev*. 2011;25(1):51–63.
21. Halder G, Dupont S, Piccolo S. Transduction of mechanical and cytoskeletal cues by YAP and TAZ. *Nat Rev Mol Cell Biol*. 2012;13(9):591–600.
22. Aragona M, et al. A mechanical checkpoint controls multicellular growth through YAP/TAZ regulation by actin-processing factors. *Cell*. 2013;154(5):1047–1059.
23. Hagerling R, Pollmann C, Kremer L, Andresen V, Kiefer F. Intravital two-photon microscopy of lymphatic vessel development and function using a transgenic Prox1 promoter-directed mOrange2 reporter mouse. *Biochem Soc Trans*. 2011;39(6):1674–1681.
24. Bazigou E, et al. Integrin-α9 is required for fibronectin matrix assembly during lymphatic valve morphogenesis. *Dev Cell*. 2009;17(2):175–186.
25. Lutter S, Xie S, Tatin F, Makinen T. Smooth muscle-endothelial cell communication activates Reelin signaling and regulates lymphatic vessel formation. *J Cell Biol*. 2012;197(6):837–849.
26. Kanady JD, Dellinger MT, Munger SJ, Witte MH, Simon AM. Connexin37 and Connexin43 deficiencies in mice disrupt lymphatic valve development result in lymphatic disorders including lymphedema chylothorax. *Dev Biol*. 2011;354(2):253–266.
27. Baluk P, et al. Functionally specialized junctions between endothelial cells of lymphatic vessels. *J Exp Med*. 2007;204(10):2349–2362.
28. Taylor RC, Cullen SP, Martin SJ. Apoptosis: controlled demolition at the cellular level. *Nat Rev Mol Cell Biol*. 2008;9(3):231–241.
29. Piccolo S, Cordenonsi M, Dupont S. Molecular pathways: YAP and TAZ take center stage in organ growth and tumorigenesis. *Clin Cancer Res*. 2013;19(18):4925–4930.
30. Johnson R, Halder G. The two faces of Hippo: targeting the Hippo pathway for regenerative medicine and cancer treatment. *Nat Rev Drug Discov*. 2014;13(1):63–79.
31. Zhao B, et al. Inactivation of YAP oncoprotein by the Hippo pathway is involved in cell contact inhibition and tissue growth control. *Genes Dev*. 2007;21(21):2747–2761.
32. Shen Z, Stanger BZ. YAP regulates S-phase entry in endothelial cells. *PLoS One*. 2015;10(1):e0117522.
33. Conway DE, Schwartz MA. Flow-dependent cellular mechanotransduction in atherosclerosis. *J Cell Sci*. 2013;126(pt 22):5101–5109.
34. Kriederman BM, et al. FOXC2 haploinsufficient mice are a model for human autosomal dominant lymphedema-distichiasis syndrome. *Hum Mol Genet*. 2003;12(10):1179–1185.
35. Bazigou E, et al. Genes regulating lymphangiogenesis control venous valve formation and maintenance in mice. *J Clin Invest*. 2011;121(8):2984–2992.
36. Stanczuk L, et al. cKit lineage hemogenic endothelium-derived cells contribute to mesenteric lymphatic vessels. *Cell Rep*. 2015; S2211-1247(15)00172-2.
37. Srinivas S, et al. Cre reporter strains produced by targeted insertion of EYFP and ECFP into the ROSA26 locus. *BMC Dev Biol*. 2001;1:4.
38. Simon AM, Goodenough DA, Li E, Paul DL. Female infertility in mice lacking connexin 37. *Nature*. 1997;385(6616):525–529.
39. Davis MJ, Scallan JP, Wolpers JH, Muthuchamy M, Gashev AA, Zawieja DC. Intrinsic increase in lymphangion muscle contractility in response to elevated afterload. *Am J Physiol Heart Circ Physiol*. 2012;303(7):H795–H808.
40. Scallan JP, Wolpers JH, Davis MJ. Constriction of isolated collecting lymphatic vessels in response to acute increases in downstream pressure. *J Physiol*. 2013;591(pt 2):443–459.
41. Dimova I, et al. Inhibition of Notch signaling induces extensive intussusceptive neo-angiogenesis by recruitment of mononuclear cells. *Angiogenesis*. 2013;16(4):921–937.
42. Norrmen C, et al. Liprin (β)1 is highly expressed in lymphatic vasculature is important for lymphatic vessel integrity. *Blood*. 2010;115(4):906–909.
43. Ivanov KI, et al. Phosphorylation regulates FOXC2-mediated transcription in lymphatic endothelial cells. *Mol Cell Biol*. 2013;33(19):3749–3761.